Nonidentical twin bands in doubly odd ^{170}Lu

G. Levinton,[1] A. J. Kreiner,[1,2,4] M. A. Cardona,[1,2] M. E. Debray,[1,2] D. Hojman,[1,2,4] J. Davidson,[3,4] G. Martí,[1] A. Burlón,[1,2] M. Davidson,[3,4] D. R. Napoli,[5] M. De Poli,[5] D. Bazzacco,[6] N. Blasi,[7] S. M. Lenzi,[6] G. Lo Bianco,[7] C. Rossi Alvarez,[6] and V. R. Vanin[8]

[1]*Departamento de Física, Comisión Nacional de Energía Atómica, Argentina*
[2]*Escuela de Ciencia y Tecnología, Universidad de San Martín, Argentina*
[3]*Departamento de Física, FCEyN, Universidad de Buenos Aires, Argentina*
[4]*CONICET, Buenos Aires, Argentina*
[5]*INFN, Laboratori Nazionali di Legnaro, Legnaro, Italy*
[6]*Dipartimento di Fisica, Sezione di Padova, Padova, Italy*
[7]*Dipartimento di Fisica and INFN, Sezione di Milano, Milano, Italy*
[8]*Instituto de Fisica, Universidade de São Paulo, Brazil*

(Received 4 January 1999; published 9 September 1999)

The doubly odd nucleus ^{170}Lu has been studied using the ^{164}Dy(^{11}B,5n) reaction at 63 MeV bombarding energy. A near yrast level scheme was constructed comprising 11 rotational bands. Among them, the $\tilde{\pi}h_{9/2} \otimes \tilde{\nu}i_{13/2}$ staggered semidecoupled structure has been established up to $I = 30\hbar$. The doubly decoupled band $\tilde{\pi}h_{9/2} \otimes \tilde{\nu}\frac{1}{2}^-[521]$ and a Newby shifted $K=0$ band were also found. A set of three bands resembles a band structure present in the neighboring odd-*A* isotopes. One of these shows a striking similarity in transition energies to the $\tilde{\pi}7/2^+[404]$ band in ^{171}Lu and hence this pair has been cataloged as *twin bands*. However, their extracted moments of inertia appear to be very different and therefore they cannot be considered identical bands in the usual sense. [S0556-2813(99)00509-9]

PACS number(s): 21.10.Re, 21.60.Ev, 23.20.Lv, 27.70.+q

I. INTRODUCTION

The study of doubly odd nuclei has provided, for at least two decades now [1–8], a fruitful ground for the discovery and discussion of a number of interesting nuclear structure features. One recurrent theme [1–4] has been the attempt to establish a general classification scheme for the coupling modes of two nonidentical valence nucleons, leading to semidecoupled [1,4], doubly decoupled [4,5] and compressed structures [2]. Other phenomena which were discovered along the way comprised signature inversion [6,7] and identical bands [8]. This last concept referred to two bands of strikingly similar transition energies in neighboring odd-mass and doubly odd isotopes, namely the $\tilde{\pi}\frac{7}{2}^+[404] \otimes \tilde{\nu}\frac{1}{2}^-[521]$ structure in ^{174}Lu and the $\tilde{\pi}\frac{7}{2}^+[404]$ band in ^{173,175}Lu. This subject is also reexamined in this work. More recently, with the advent of powerful γ-ray detector arrays, a large amount of high-quality data became available revealing new examples of structures and subjecting ideas and models to increasingly stringent tests. One of the most exciting issues brought into focus with the development of large Ge detector arrays was the finding of identical bands in the superdeformed regime [9,10]. The term *identical* refers currently to bands having equal moments of inertia while the term *twin bands* stands for structures with equal transition energies. In the superdeformed regime ($I \simeq 40\hbar$ and $\beta \simeq 0.6$) it is possible to see that twin bands are also identical. The question arises, however, if this statement is also valid in the normal deformation regime. The present study of ^{170}Lu is framed into the above context and is likely to provide an example for nonidentical twin bands. The doubly odd nucleus ^{170}Lu has been examined [11] using the GASP detector array at the Legnaro Tandem Facility. Eleven rotational bands, some up to high spins, were constructed on the basis of the experimental data. An analysis of directional correlation orientation (DCO) ratios, $B(M1)/B(E2)$ ratios, ground to *S*-band crossing frequencies and structure systematics in this region of the periodic table have been used to identify the structures on which the rotational bands are based. A cranking model has been used to extract the inertia parameters and rotational alignments for all bands. All bands show a fairly good additivity [12] of their parameters (within 5% for $\mathcal{T}_0$). A two-quasiparticles-plus-rotor model [1,13] with a variable moment of inertia (VMI) [14] has been applied to the special cases of doubly decoupled bands, semidecoupled bands, and Newby [15] shifted $K=0$ bands.

II. EXPERIMENTS AND RESULTS

A. Measurements

High-spin states of ^{170}Lu were populated through the ^{164}Dy(^{11}B,5*n*) reaction at 63 MeV bombarding energy. The beam was provided by the Tandem XTU accelerator at Legnaro National Laboratory, Italy, and γ rays emitted by the reaction residues were detected using the GASP array [16], which consisted for this coincidence experiment of 40 Compton suppressed large volume Ge detectors and an 80 BGO multiplicity filter, providing the sum-energy and γ-ray multiplicity used to select the different reaction channels. All the events (near 10^9) were recorded with the condition that at least three suppressed Ge and three inner multiplicity filter

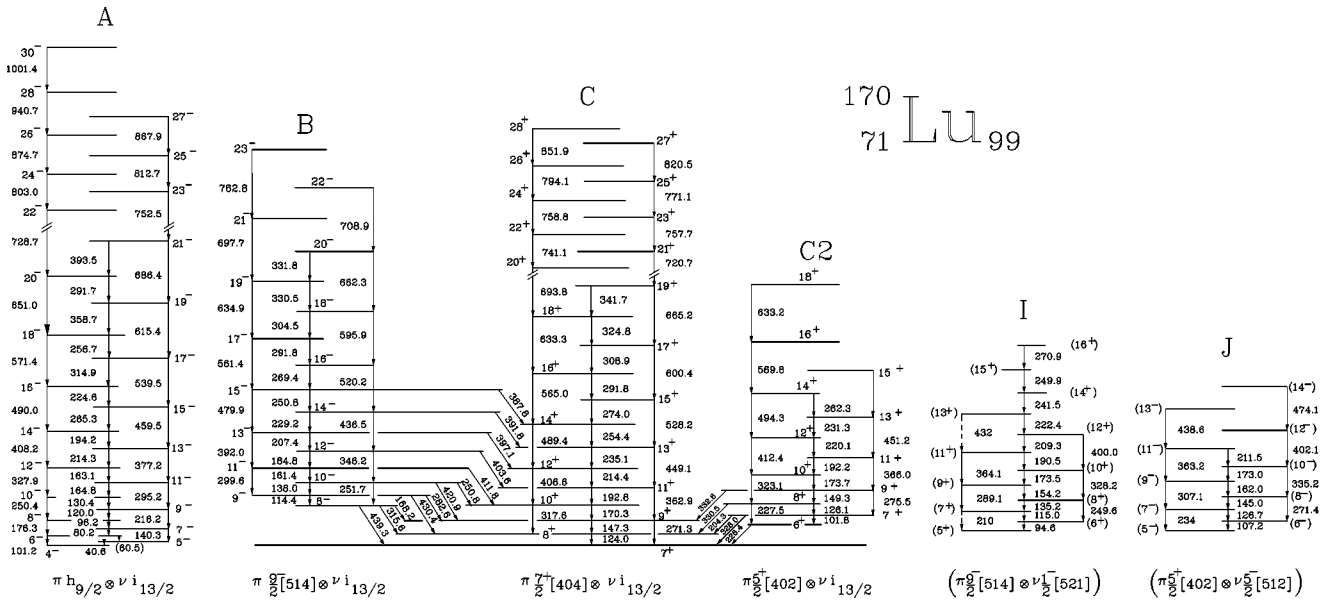

FIG. 1. Partial level scheme of the nucleus ^{170}Lu obtained in this work. From left to right are shown bands *A*, *B*, *C*, *C*2, *I*, and *J*. Tentative assignments are given between parenthesis.

detectors were fired. The data corresponding to Ge energies were sorted into fully symmetrized matrices and cubes. The large number of triple coincidences allowed the possibility of generating matrices gated by transitions in different bands of ^{170}Lu and of obtaining very clean double-gated spectra. A complementary experiment was carried out at Tandar Laboratory, Buenos Aires, using the same target and reaction and a detection system composed by one planar Ge detector and an 11-element multiplicity filter with the purpose of measuring halflives in the nanosecond range. The 98.5 keV line shows a halflife $T_{1/2}=2.6(2)$ ns, clearly indicating that is an out-of-band transition. On the other hand, an upper limit of 1 ns, consistent with a prompt character, was obtained for the 132.2 keV γ ray which depopulates the (3^+) state of band *F*.

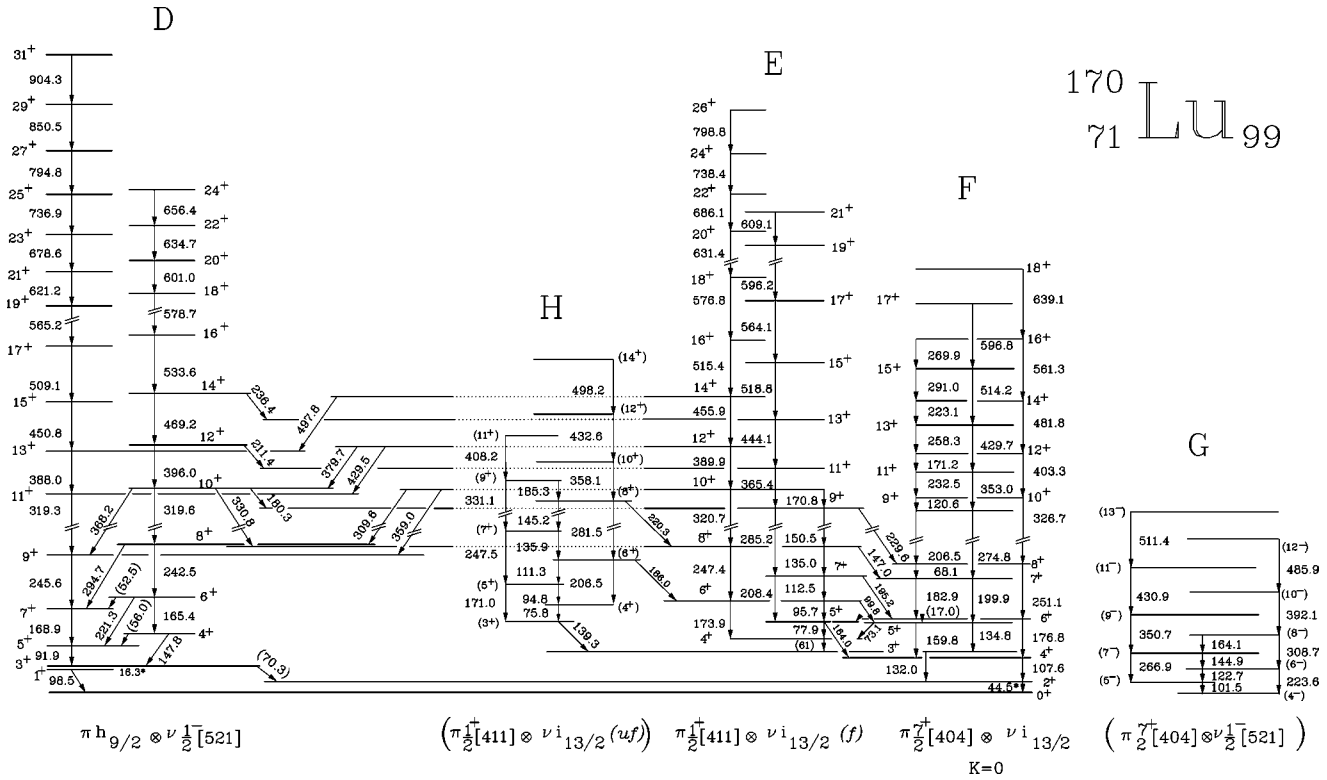

FIG. 2. Partial level scheme of the nucleus ^{170}Lu obtained in this work. Bands *D*, *H*, *E*, *F*, and *G* are shown from left to right. Tentative assignments are given between parenthesis.

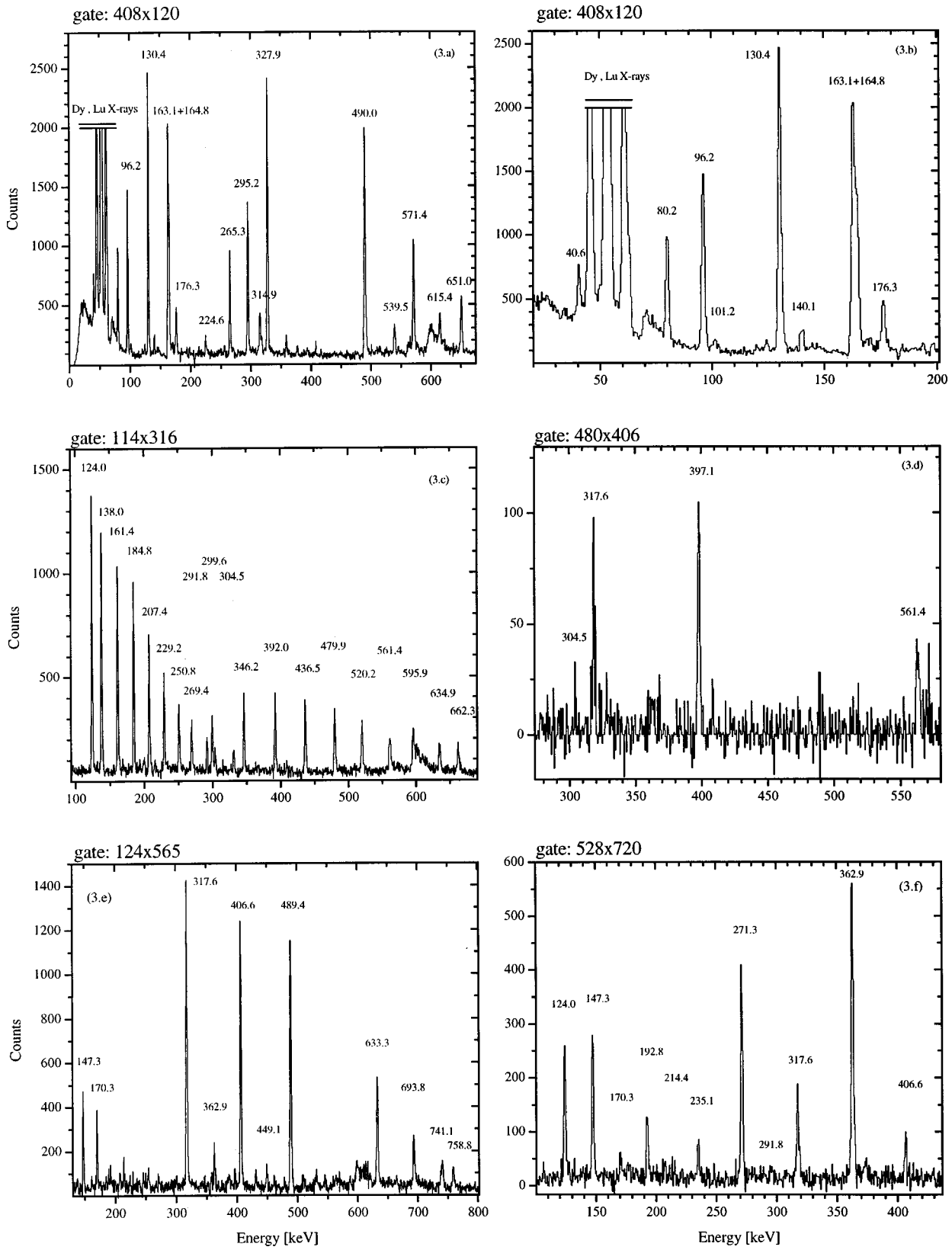

FIG. 3. (a) Spectrum in coincidence with the 408.2 and 120.0 keV γ rays. (b) Enlargement of the low-energy portion of the spectrum (a). (c) Spectrum in coincidence with the 114.4 and 315.6 keV γ rays. (d) Enhanced linking transitions by setting a gate on the 406.6 keV line in the matrix in coincidence with the 479.9 keV transition. (e) Coincidence spectrum showing the quadrupolar cascade of band *C*. (f) Enlargement of a coincidence spectrum enhancing the dipolar transitions in band *C*.

B. Level scheme of ^{170}Lu

The level scheme for ^{170}Lu deduced from the data obtained here is shown in Figs. 1 and 2. Good agreement was reached with the previously known data [17] obtained from the decay of ^{170}Hf where the ground state was observed to be $I^{\pi}=0^{+}$ and assigned to the $\tilde{\pi}\frac{7}{2}^{+}[404]\otimes i_{13/2}(\frac{7}{2}^{+}[633])$, antiparallel coupling. Figure 3 shows examples of the high-quality coincidence spectra of the Ge detectors gated on pairs of transitions belonging to the same band or two different bands to enhance the linking transitions between them. A first energy calibration was made with Eu and Ba radioactive sources. In-beam spectra at different angles were Doppler matched. A further energy correction was made using on-line data, in particular known ^{170}Yb and ^{167}Tm quadrupole transitions [18,19] that were also populated in the experiment through $p4n$ and $\alpha 4n$ reactions, respectively. The neighboring odd-Lu isotopes were populated as well and very good agreement was obtained with the already known transition energies [20,21]. The multipolarities were inferred from intensity balance, in-band analysis (matching of pairs of $\Delta I=1$ transitions to their corresponding $\Delta I=2$ and coincidence conditions) and directional correlation orientation (DCO) analysis, which has been done using the data collected by the detectors placed at $\theta_1=34.5^{o}$ and $\theta_2=90^{o}$. The ratios $I_{\gamma_x,\theta_1}(\gamma_0,\theta_2)/I_{\gamma_x,\theta_2}(\gamma_0,\theta_1)$, where $I_{\gamma_x,\theta_1}(\gamma_0,\theta_2)$ is the intensity at angle θ_1 of the observed γ ray γ_x in coincidence with the line γ_0 at θ_2, were compared to the ones calculated theoretically [22]. A complete list of ^{170}Lu gamma ray energies can be found in Table I separated by band, together with their corresponding experimental DCO ratios, assigned multipolarities, and the method used to assign them. Further experimental information was obtained by in band branching ratios for a given level. This quantity can be compared with the calculated effective branching ratios:

$$\left[\left(\frac{I_\gamma}{E_\gamma^3}\right)_{\Delta I=1}\times\left(\frac{E_\gamma^5}{I_\gamma}\right)_{\Delta I=2}\right]_{\exp}=\left[\frac{B(M1)}{B(E2)}(1+\delta^2)\right]_{\mathrm{th}},$$

where $B(M1)/B(E2)$ are the pure branching ratios and δ denotes the $E2$ to $M1$ mixing coefficient for an in-band $\Delta I=1$ transition. The expression used for the theoretical calculation is given in Ref. [23]. A complete list of level spins with their corresponding experimental effective branching ratios can be found in Table II.

1. Band A

This band receives the strongest population in our experiment. The predominant $M1$ character of the $\Delta I=1$ transitions follows from DCO analysis and intensity balance considerations. The difference between the sum of two $\Delta I=1$ transition energies and the corresponding $\Delta I=2$ crossover energies is within the final experimental uncertainty. The 60.5 keV transition (shown in parenthesis in Fig. 1) was most likely not observed because it is masked by the K_β Lu x rays. Its existence was inferred from the observation of the spectra in coincidence with the 140.3 and 101.2 keV transitions and from the distorted x-ray intensity relations in the spectra in coincidence with the 60.5 keV line. The spins and parity assignments of this band are based on systematics [24] and theoretical assumptions, which are explained further in the discussion section.

2. Bands B, C, and C2

The striking similarity of this structure with the one observed in the neighboring ^{169,171}Lu isotopes (see Sec. III C) allowed a rapid identification of in-band quadrupole and dipole transitions and linking γ rays. This identification was then confirmed by a DCO analysis. A detailed DCO study of the three linking transitions that depopulate the level below the 114.4 keV γ ray fixes the spin difference between the two band heads to be $|I_{0B}-I_{0C}|=1$. The $E1$ multipolarity of the 168.2 keV linking transition was extracted from an intensity balance analysis. This fact leads to opposite relative parity for the two bands. The same procedure revealed the $M1(E2)$ character of the 226.4 and 204.3 keV γ-rays that link bands C and $C2$. The absolute spins and parities of these three bands were based on theoretical assumptions, which are explained in the discussion section. In Fig. 9 the striking similarity between the transition energies of the structure composed of bands *B*, *C*, and *C*2 and the one observed for the odd-proton excitations in ^{169,171}Lu composed by $\tilde{\pi}\frac{9}{2}^{-}[514]$, $\tilde{\pi}\frac{5}{2}^{+}[402]$ and (more impressively) $\tilde{\pi}\frac{7}{2}^{+}[404]$ becomes apparent. The high degree of similarity of the γ ray energies (reinforced by the fact that the levels of ^{169,171}Lu are also populated in this experiment and that the same calibration applies to all nuclei) leads us to characterize these pairs of bands as twins.

3. Bands D, H, E, and F

The observed transitions for both favored and unfavored components of band *D* have the characteristics of stretched quadrupoles. The existence of the 56.0 keV transition has been inferred from the distorted Lu x-ray intensity relations. The accidental degeneracy of different levels determines the relative spins and parities of bands *D* and *E* on one side and bands *E* and *F* on the other. An intensity balance analysis for the low-energy links (180.3, 211.2, and 236.3 keV from band *D* to *E* and 99.8 and 164.0 keV from band *E* to *F*) resulted in an $M1/E2$ mixture for all transitions. A DCO ratio analysis suggests that the 220.3 keV transition that links bands *H* and *E* does not change the spin. This fact hence suggests the relative spin of band *H* with respect to band *E*. The 70.3 keV transition was observed by subtracting the spectrum in coincidence with the 245.6 and 168.9 keV lines from the one in coincidence with the 245.6 and 98.5 keV γ rays, both normalized to the intensity of the 91.9 keV line. The resulting spectrum can be seen in Fig. 4. Both 98.5 and 70.3 keV γ rays depopulate band *D* and the existence of other highly converted low-energy hidden transitions between the upper band members and these γ rays cannot be excluded. In particular a 16.3 keV transition can be placed below the

TABLE I. List of γ-ray energies, DCO ratios, assigned multipolarities, and method used to assign them (DCO, IB is the intensity balance, II is the in-band sum-energy analysis, see text for explanation) separated by band. Unless otherwise noted the DCO ratios were extracted using a quadrupole line as the gating transition.

	E_γ (keV)	DCO	Mult.	Method		E_γ (keV)	DCO	Mult.	Method
Band *A*	40.56(7)	*M*1/*E*2	II			304.5(1)		*M*1/*E*2	II
	60.5(5)	*M*1/*E*2	II			330.47(6)		*M*1/*E*2	II
	80.17(4)	0.77(5)	*M*1/*E*2	DCO-II		331.80(6)		*M*1/*E*2	II
	96.16(4)	0.62(3)	*M*1/*E*2	DCO-II		346.15(4)	1.07(5)	*E*2	DCO-II
	101.2(1)		*E*2	II		391.96(5)	1.4(1)	*E*2	DCO-II
	120.05(3)	0.55(3)	*M*1/*E*2	DCO-II		436.48(7)	0.88(5)	*E*2	DCO-II
	130.37(3)	0.43(3)	*M*1/*E*2	DCO-II		479.92(9)		*E*2	II
	140.13(3)		*E*2	II		520.2(1)	0.8(1)	*E*2	DCO-II
	163.13(3)	0.45(3)	*M*1/*E*2	DCO-II		561.4(2)	1.01(5)	*E*2	DCO-II
	164.82(3)	0.43(3)	*M*1/*E*2	DCO-II		595.9(2)		*E*2	II
	176.30(4)	0.95(5)	*E*2	DCO-II		634.9(2)		*E*2	II
	194.21(3)	0.44(3)	*M*1/*E*2	DCO-II		662.3(3)		*E*2	II
	214.31(4)	0.41(3)	*M*1/*E*2	DCO-II		697.7(4)		*E*2	II
	216.22(4)	0.98(5)	*E*2	DCO-II		708.9(5)		*E*2	II
	224.61(4)	0.45(3)	*M*1/*E*2	DCO-II		762.8(5)		*E*2	II
	250.40(3)	0.84(5)	*E*2	DCO-II	Links	168.20(5)		*E*1	IB
	256.72(7)	0.39(5)	*M*1/*E*2	DCO-II	*B* to *C*	250.77(4)		*E*1	II
	265.33(7)	0.38(5)	*M*1/*E*2	DCO-II		282.70(4)		*E*1	II
	291.7(5)	0.4(1)	*M*1/*E*2	DCO-II		315.63(4)	$0.86(5)^{M1}$	*E*1	DCO-IB
	295.21(3)	0.93(5)	*E*2	DCO-II		387.75(7)		*E*1	II
	314.91(6)	0.44(3)	*M*1/*E*2	DCO-II		391.82(7)		*E*1	II
	327.90(3)	1.00(3)	*E*2	DCO-II		397.10(9)		*E*1	II
	358.73(5)	0.55(5)	*M*1/*E*2	DCO-II		403.60(6)		*E*1	II
	377.22(4)	1.00(3)	*E*2	DCO-II		411.83(7)		*E*1	II
	393.48(6)		*M*1/*E*2	II		420.88		*E*1	II
	408.25(5)	1.07(5)	*E*2	DCO-II		430.4(1)		*E*1	II
	459.5(1)	1.03(5)	*E*2	DCO-II		439.3(2)	$0.96(8)^{M1}$	*E*1	DCO-II
	490.02(9)	1.1(1)	*E*2	DCO-II	Band	124.01(6)	1.04(5)	*M*1/*E*2	DCO-II
	539.5(1)	1.03(5)	*E*2	DCO-II	*C*				
	571.4(2)	1.13(7)	*E*2	DCO-II		147.35(4)	1.06(5)	*M*1/*E*2	DCO-II
	615.4(2)	1.05(7)	*E*2	DCO-II		170.28(5)	1.10(5)	*M*1/*E*2	DCO-II
	651.0(3)	1.3(1)	*E*2	DCO-II		192.75(5)	0.58(5)	*M*1/*E*2	DCO-II
	686.4(2)		*E*2	II		214.4(1)	0.82(8)	*M*1/*E*2	DCO-II
	728.7(3)		*E*2	II		235.11(6)		*M*1/*E*2	II
	752.5(4)		*E*2	II		254.42(8)	0.99(7)	*M*1/*E*2	DCO-II
	803.0(5)		*E*2	II		271.3(2)	0.95(5)	*E*2	DCO-II
	867.9(7)		*E*2	II		274.0(1)		*M*1/*E*2	II
	874.7(6)		*E*2	II		291.76(4)		*M*1/*E*2	II
	940.7(7)		*E*2	II		308.89(6)		*M*1/*E*2	II
	1001(2)		*E*2	II		317.58(4)	0.98(4)	*E*2	DCO-II
Band *B*	114.43(4)		*M*1/*E*2	II		362.92(5)	1.13(5)	*E*2	DCO-II
	137.99(5)	1.03(5)	*M*1/*E*2	DCO-II		406.65(9)	0.88(7)	*E*2	DCO-II
	161.45(3)	1.01(5)	*M*1/*E*2	DCO-II		449.1(1)	0.89(7)	*E*2	DCO-II
	184.76(2)	0.83(5)	*M*1/*E*2	DCO-II		489.37(9)	0.93(7)	*E*2	DCO-II
	207.41(4)	0.84(5)	*M*1/*E*2	DCO-II		528.2(1)		*E*2	II
	229.17(3)	0.80(5)	*M*1/*E*2	DCO-II		569.8(2)		*E*2	II
	250.80(4)		*M*1/*E*2	II		600.3(2)		*E*2	II
	251.7(1)	0.83(5)	*E*2	DCO-II		633.3(2)		*E*2	II
	269.42(4)	0.69(5)	*M*1/*E*2	DCO-II		665.2(3)		*E*2	II
	291.80(3)	0.96(5)	*M*1/*E*2	II		693.8(3)		*E*2	II
	299.6(1)	0.94(5)	*E*2	DCO-II		720.7(3)		*E*2	II

TABLE I. (*Continued*).

	E_γ (keV)	DCO	Mult.	Method		E_γ (keV)	DCO	Mult.	Method
	741.1(4)		$E2$	II		850.5(5)		$E2$	II
	757.7(4)		$E2$	II		904.3(7)		$E2$	II
	758.8(4)		$E2$	II	Links	180.34(5)		$M1/E2$	
Band $C2$	101.78(6)		$M1/E2$	II	D to E	211.38(6)		$M1/E2$	IB
	126.14(3)		$M1/E2$	II		236.40(6)		$M1/E2$	IB
	149.32(3)		$M1/E2$	II		309.65(5)		$E2$	II
	173.68(5)		$M1/E2$	II		330.82(8)		$E2$	II
	192.19(6)		$M1/E2$	II		359.0(2)		$E2$	II
	220.11(7)		$M1/E2$	II		379.70(6)		$E2$	II
	227.54(3)		$E2$	II		429.5(3)		$E2$	II
	231.34(6)		$M1/E2$	II		497.8(3)		$E2$	II
	262.35(5)		$M1/E2$	II	Band $E3$	95.68(7)		$M1/E2$	IB
	275.52(4)		$E2$	II		112.48(9)		$M1/E2$	IB
	323.06(6)		$E2$	II		134.96(7)		$M1/E2$	II
	366.05(4)		$E2$	II		150.50(9)		$M1/E2$	II
	412.42(5)		$E2$	II		173.95(7)	0.99(5)	$E2$	DCO
	451.2(1)		$E2$	II		208.38(8)	1.02(5)	$E2$	DCO
	494.3(2)		$E2$	II		247.65(5)		$E2$	II
	569.8(2)		$E2$	II		285.20(6)	0.97(5)	$E2$	DCO
	633.2(4)		$E2$	II		320.77(6)		$E2$	II
Links	204.4(2)		$M1/E2$	IB		365.41(5)		$E2$	II
$C2$ to C	226.36(3)		$M1/E2$	IB		389.89(8)		$E2$	II
	328.2(2)		$M1/E2$	II		444.15(7)		$E2$	II
	330.5(3)		$M1/E2$	II		455.97(9)		$E2$	II
	332.6(1)		$M1/E2$	II		515.4(1)		E	II
Band D	70.36(6)		$M1/E2$	[17]		518.8(1)		$E2$	II
	91.95(5)	0.97(5)	$E2$	DCO-IB		564.1(2)		$E2$	II
	98.55(5)	0.74(5)	$M1/E2$	DCO-IB- [17]		576.8(2)		$E2$	II
	147.75(3)			II		596.2(2)		$E2$	II
	165.37(4)	1.01(5)	$E2$	DCO-IB		609.1(3)		$E2$	II
	168.88(3)	0.87(5)	$E2$	DCO-IB		631.3(2)		$E2$	II
	221.29(3)	1.3(2)	$M1/E2$	DCO-IB		686.0(3)		$E2$	II
	242.5(1)	0.83(5)	$E2$	DCO-IB		738.4(4)		$E2$	II
	245.63(3)	0.91(5)	$E2$	DCO-IB		798.8(5)		$E2$	II
	294.71(5)	1.4(2)	$M1/E2$	DCO-IB	Links	61(1)		$M1/E2$	II
	319.28(4)	1.02(5)	$E2$	DCO-IB	E to F	99.84(7)		$M1/E2$	IB
	319.61(4)	1.11(6)	$E2$	DCO-IB		147.0(1)		$M1/E2$	II
	368.16(6)		$M1/E2$	II		164.02(4)		$M1/E2$	IB
	387.98(4)		$E2$	II		195.18(4)	0.55(3)	$M1/E2$	DCO-II
	396.00(4)	1.10(7)	$E2$	DCO		229.58(4)	0.65(4)	$M1/E2$	DCO-II
	450.84(8)		$E2$	II	Band F	68.08(5)		$M1/E2$	II
	469.18(8)		$E2$	II		107.58(4)	0.92(5)	$E2$	DCO
	509.1(1)		$E2$	II		120.61(4)	0.45(5)	$M1/E2$	DCO-II
	533.6(1)		$E2$	II		132.04(7)	0.5(1)	$M1/E2$	DCO-IB- [17]
	565.2(2)		$E2$	II		134.8(2)		$E2$	II
	578.7(2)		$E2$	II		159.83(5)		$M1/E2$	IB
	601.0(2)		$E2$	II		171.19(3)	0.96(5)	$M1/E2$	II
	621.2(2)		$E2$	II		176.77(3)	1.08(5)	$E2$	DCO
	634.7(3)		$E2$	II		182.93(3)	0.35(3)	$M1/E2$	DCO
	656.4(4)		$E2$	II		199.9(1)		$E2$	II
	678.6(3)		$E2$	II		206.47(3)	0.75(5)	$M1/E2$	DCO
	736.9(4)		$E2$	II		223.15(5)		$M1/E2$	II
	794.8(5)		$E2$	II		232.47(4)	0.45(4)	$M1/E2$	DCO

TABLE I. (*Continued*).

	E_γ (keV)	DCO	Mult.	Method		E_γ (keV)	DCO	Mult.	Method
	251.08(4)	1.04(4)	$E2$	DCO		408.6(1)		$E2$	II
	258.35(6)		$M1/E2$	II		432.6(1)		$E2$	II
	269.91(6)		$M1/E2$	II	Links	139.3(2)		$M1/E2$	IB
	274.78(8)	1.16(9)	$E2$	DCO	H to E, F	186.0(2)		$M1/E2$	II
	291.02(8)		$M1/E2$	II		220.3(3)		$M1/E2$	IB
	326.75(6)	0.91(5)	$E2$	DCO	Band I	94.6(1)		$M1/E2$	
	353.03(5)	0.9(1)	$E2$	DCO		115.0(1)		$M1/E2$	
	403.28(9)	1.03(4)	$E2$	DCO		135.2(2)		$M1/E2$	
	429.7(1)		$E2$	II		154.2(2)		$M1/E2$	
	481.8(1)		$E2$	II		173.5(2)		$M1/E2$	
	514.2(2)		$E2$	II		190.5(2)		$M1/E2$	
	561.3(2)		$E2$	II		209.3(3)		$M1/E2$	
	596.8(2)		$E2$	II		210(1)		$E2$	
	639.1(3)		$E2$	II		222.4(2)		$M1/E2$	
Band G	101.6(3)		$M1/E2$	II		241.5(3)		$M1/E2$	
	122.4(1)		$M1/E2$	II		249.6(5)		$E2$	
	145.0(1)		$M1/E2$	II		249.9(3)		$M1/E2$	
	164.5(4)		$M1/E2$	II		270.9(3)		$M1/E2$	
	223.2(4)		$E2$	II		289.1(3)		$E2$	
	267.4(1)		$E2$	II		328.2(3)		$E2$	
	309.0(1)		$E2$	II		364.1(3)		$E2$	
	350.7(2)		$E2$	II		400.0(5)		$E2$	
	392.1(5)	1.0(1)	$E2$	DCO-II		432(1)		$E2$	
	430.9(5)		$E2$	II	Band J	107.2(1)		$M1/E2$	
	485.7(1)		$E2$	II		126.7(1)		$M1/E2$	
	511(2)		$E2$	II		145.0(2)		$M1/E2$	
Band H	75.8(1)		$M1/E2$	II		162.0(2)		$M1/E2$	
	94.8(2)	0.6(2)	$M1/E2$	DCO		173.0(2)		$M1/E2$	
	11.3(2)	0.6(2)	$M1/E2$	DCO		211.5(3)		$M1/E2$	
	135.89(5)		$M1/E2$	II		234(1)		$E2$	
	145.2(2)		$M1/E2$	II		271.4(3)		$E2$	
	171.0(2)		$E2$	II		307.1(3)		$E2$	
	185.3(3)		$M1/E2$	II		335.2(3)		$E2$	
	206.5(3)		$E2$	II		363.2(3)		$E2$	
	247.71(6)		$E2$	II		402.1(4)		$E2$	
	281(1)		$E2$	II		438.6(4)		$E2$	
	332(2)		$E2$	II		474.1(5)		$E2$	
	358.21(7)		$E2$	II					

91.9 keV line to reach agreement with the previously known ^{170}Lu level scheme [17]. In this way the three bands are connected to the ground-state level below the 98.5 keV transition. The 132.0 keV γ ray does not show a halflife greater than 1 ns (detection limit of this experiment) and hence has been treated as a prompt γ ray that belongs to band F, as previously observed confirming the proposed scheme.

4. Bands G, I, and J

These structures appear as isolated dipole bands. The spins and parities are completely based on theoretical assumptions and have tentative character.

III. DISCUSSION

The identification of proton and neutron orbitals involved in the rotational bands of ^{170}Lu was done on the basis of the coupling schemes proposed by Kreiner *et al.* [3] For the doubly odd nucleus ^{170}Lu the zero-order level scheme was constructed adding the experimental band-head energies extracted from neighboring odd proton and neutron isotopes (and neglecting the residual interaction which can split the $K^{>}_{<}=|\Omega_p \pm \Omega_n|$ states according to the Gallagher-Moszkowski coupling rules [25], see Table III). As a helpful tool to qualitatively characterize the kind of coupling

TABLE II. Effective branching ratios extracted from experimental data and separated by band as a function of spin I of the emitting state.

Spin ($\hbar$)	$\left[\frac{B(M1)}{B(E2)}\right]_{\text{eff}}$ (e^2b)	Spin ($\hbar$)	$\left[\frac{B(M1)}{B(E2)}\right]_{\text{eff}}$ (e^2b)
Band A		16	0.26(4)
7	0.26(3)	17	0.14(4)
8	0.35(3)	Band $C2$	
9	0.29(2)	9	0.6(1)
10	0.31(1)	10	0.8(2)
11	0.27(1)	11	0.8(4)
12	0.36(1)	12	0.1(1)
13	0.26(1)	Band E	
14	0.29(1)	6	0.02(2)
15	0.26(2)	7	0.2(1)
16	0.24(1)	8	0.04(2)
17	0.19(1)	9	0.5(3)
18	0.20(2)	10	0.05(3)
19	0.19(2)	Band F	
Band B		7	0.4(1)
10	1.5(2)	8	0.7(1)
11	1.1(1)	19	0.5(1)
12	0.96(9)	12	4.8(9)
13	0.65(6)	13	1.1(2)
14	0.68(7)	14	0.7(1)
15	0.79(9)	Band G	5 0.4(1)
16	0.8(1)	6	0.17(4)
17	0.8(2)	Band H	(5) 0.4(2)
18	0.5(1)	(6)	0.42(15)
Band C		(7)	0.45(15)
9	0.14(1)	Band I	(7) $>0.3(1)$
10	0.07(5)	(8)	$>0.6(2)$
11	0.15(1)	(9)	1.5(6)
12	0.07(5)	Band J	(6) 0.6(3)
13	0.14(1)	(7)	0.3(1)
14	0.03(3)	(8)	0.4(1)
15	0.08(3)	(9)	$>0.21(8)$

scheme, the parameter K_1 was extracted [this parameter is defined in [2] as $K_1=(2-x)/(x-1)$, where x is the ratio between the $(I_0+2\rightarrow I_0+1)$ and the $(I_0+1\rightarrow I_0)$ transition energies and I_0 is the band-head spin and would coincide with the K value of the band for a normal and rigid structure]. For the ^{170}Lu rotational bands found in the present work, the configuration assignments were based on systematics and on the analysis of band properties such as rotation alignments, band crossing frequencies, $B(M1)/B(E2)$ values, mixing ratios of $M1(E2)$ transitions, signature splitting, etc. In order to further explore the consistency of the structure assignments an analysis in terms of simple versions of the particle plus rotor model has been done. For each $(\Delta I=2)$ band the inertia parameters were extracted by fitting the energies of the first four quadrupole transitions to the cranking model, in order to check additivity rules.

A. The different models

In this work, the characterization of the rotational bands comes ultimately from the comparison of physically meaningful parameters extracted from the fit of experimental data to a theoretical model. The theoretical approaches have been kept as simple as possible (e.g., minimal dimensions for configuration spaces have been used) without losing the essential ingredients for a given case, in order to achieve maximum transparency in the analysis. The cranking model and simple versions of the particle plus rotor model are used to find an expression for the energy levels as a function of the total angular momentum and a set of n parameters:

$$E_{\text{th}}(I,a_1\cdots a_n). \tag{1}$$

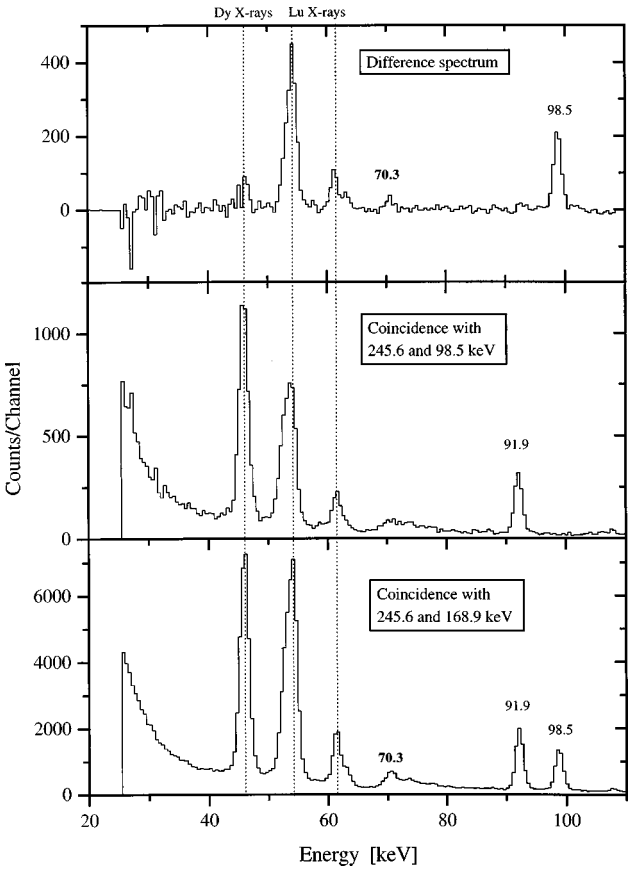

FIG. 4. (top) Subtraction spectrum of (middle), the spectrum in coincidence with the 245.6 and the 98.5 keV transitions, from (bottom), the spectrum in coincidence with the 245.6 and the 168.9 keV ones, both normalized to the intensity of the 91.9 keV γ ray. A peak at 70.3 keV arises over a nearly flat background of zero counts.

The parameters are then extracted through a correlated nonlinear least-squares fit that consists in the minimization of the function

$$\chi^2(a_1 \cdots a_n) = X^t V^{-1} X, \tag{2}$$

where X is a vector that contains the differences $E_{\rm th}(I_i,\vec{a}) - E_{\rm th}(I_i-\Delta I,\vec{a}) - E_\gamma(I_i \rightarrow I_i - \Delta I)$ ($\Delta I = 1$ or 2 depending on which transitions are used in the fit and i runs over the number of selected data points) and V is the variance matrix.

The cranking model proposed by Harris [26] is one of the most extensively used models for the description of rotational states in heavy nuclei. The rotational energy of a particular state can be written as follows:

$$E_{\rm cr}(\omega_x, \Im_0, \Im_1, i_0) = \frac{1}{2}\left(\Im_0 + \frac{3}{2}\Im_1\omega_x^2\right)\omega_x^2, \tag{3}$$

where $\Im_0, \Im_1$ are the inertia parameters, i_0 is the alignment, and ω_x is the rotational frequency. This frequency is a function of the spin I, the three parameters and the mean-square value of the projection of the total angular momentum on the symmetry axis denoted by K, which has been taken as fixed because it is strongly correlated with $\Im_0, \Im_1$, and i_0. The function $\omega_x(I, \Im_0, \Im_1, i_0)$ can be found as the physically meaningful solution of the cubic equation

$$\sqrt{I(I+1) - \langle K^2 \rangle} - i_0 = (\Im_0 + \Im_1\omega_x^2)\omega_x. \tag{4}$$

This semiclassical model assumes a nucleus with a cinematic [27] moment of inertia $\Im^{(1)} = \Im_0 + \Im_1\omega_x^2$ rotating with frequency ω_x around an axis perpendicular to the symmetry axis, and all the noncollective contributions are taken into account through i_0 on the axis of rotation and the root mean square of K on the symmetry axis. The main advantage of this model is that the same form applies for even-even, odd, and doubly odd nuclei.

The N quasiparticles plus VMI-rotor (VMI-NQPR) model Hamiltonian can be written

$$\hat{H}_{ppr} = \hat{H}_{\rm rot} + \sum_k \hat{h}_{{\rm int}_k} + \hat{V}_{\rm pn}, \tag{5}$$

where $\hat{h}_{{\rm int}_k}$ is the intrinsic Hamiltonian of the valence quasiparticles, $\hat{V}_{pn}$ is the residual interaction among them and

$$\hat{H}_{\rm rot} = \frac{1}{2\Im}\hat{R}^2 + \frac{1}{4\Im_1}(\Im - \Im_0)^2 \tag{6}$$

TABLE III. Zero-order level scheme of ^{170}Lu. Entries are $K_{<}^{>} = |\Omega_p \pm \Omega_n|$ values and zero-order energies in keV. Excitation energies correspond to the average of ^{169}Lu and ^{171}Lu for protons and to the average of ^{169}Yb and ^{171}Hf for neutrons.

	$\tilde{\nu}\Omega^\pi[Nn_3\Lambda]$	$7/2^+[633]$ ($i_{3/2}$)	$1/2^-[521]$	$5/2^-[512]$
$\tilde{\pi}\Omega^\pi[Nn_3\Lambda]$	E_ν (keV)	0.0	23.2	120.4
E_π (keV)				
$7/2^+[404]$		$0^+, 7^+$	$3^-, 4^-$	$1^-, 6^-$
0.0		0.0	23.2	120.4
$1/2^-[541]$ ($h_{9/2}$)		$3^-, 4^-$	$0^+, 1^+$	$2^+, 3^+$
50.1		50.1	73.3	170.5
$1/2^+[411]$		$3^+, 4^+$	$0^-, 1^-$	$2^-, 3^-$
152.8		152.8	176.0	273.2
$5/2^+[402]$		$1^+, 6^+$	$2^-, 3^-$	$0^-, 5^-$
240.9		240.9	264.1	361.3
$9/2^-[514]$ ($h_{11/2}$)		$1^-, 8^-$	$4^+, 5^+$	$2^+, 7^+$
454.1		454.1	477.3	574.5

TABLE IV. Parameters used (μ) in and extracted by the Nilsson calculations ($\langle s_3\rangle$, $\langle j^{\perp 2}\rangle$) and alignments ($i$) used in the semiclassical approximation of $B(M1)$ values. The alignments were extracted averaging the ones obtained from ^{169}Lu and ^{171}Lu for proton orbitals and ^{169}Yb and ^{171}Hf for neutron orbitals.

Core deformation: $\beta=0.312(5)$, $\kappa=0.05$ [a]	Orbital	$i(\hbar)$	μ [a]	$\langle s_3\rangle(\hbar)$	$\langle j^{\perp 2}\rangle(\hbar)$
	$7/2^+[404]$	0.0	0.625	-0.46	3.66
	$1/2^-[541]$	2.1	0.7	-0.08	18.88
Protons	$1/2^+[411]$	0.5	0.625	0.35	11.08
	$5/2^+[402]$	0.0	0.625	-0.45	3.17
	$9/2^-[514]$	0.4	0.7	0.46	15.37
	$7/2^+[633]$	0.7	0.448	0.37	34.62
Neutrons	$1/2^-[521]$	0.35	0.45	-0.28	13.44
	$5/2^-[512]$	0.1	0.45	0.40	11.94

[a]Values taken from Ref. [29].

is a VMI Hamiltonian, where $\hat{R}=\hat{I}-\hat{J}$ is the collective angular momentum. The second term of the equation comes from the variable character of the moment of inertia and takes into account the amount of energy spent to change it from the static ground-state value $\mathfrak{I}_0$. The moment of inertia $\mathfrak{I}$ for a particular rotational level can be found from the physically meaningful solution of the cubic equation

$$\mathfrak{I}^3-\mathfrak{I}_0\mathfrak{I}^2-\mathfrak{I}_1\langle\hat{R}^2\rangle=0, \tag{7}$$

which comes from the condition of minimum energy (equilibrium value) and $\langle\hat{R}^2\rangle$ is the mean-square value of $\hat{R}$. It should be mentioned that the inertia parameters $\mathfrak{I}_0$ and $\mathfrak{I}_1$ are not necessarily equal in both models. The number of parameters and the explicit form of the eigenvalues of $\hat{H}$ as a function of these parameters and I depends on the selected number of particles outside the core and on how many quasiparticle states one includes in the basis. The ground-state band of an even-even nucleus can be taken as a rotating nonrigid core, and hence the energy of the levels is easily calculated as

$$E_{e\text{-}e}(I)=\frac{1}{2\mathfrak{I}}I(I+1)+\frac{1}{4\mathfrak{I}_1}(\mathfrak{I}-\mathfrak{I}_0)^2. \tag{8}$$

This particular case is analytically equivalent to the cranking model, as was pointed out in [14]. For an odd nucleus one can take one quasiparticle outside the even-even core in a pure $K=\Omega$ asymptotic Nilsson [28] state (the predictions will not be very accurate in cases of $h_{9/2}$ or $i_{13/2}$ parentage or more generally for high-j parentage orbits where Coriolis matrix elements are large) leading to the expression of the energy levels

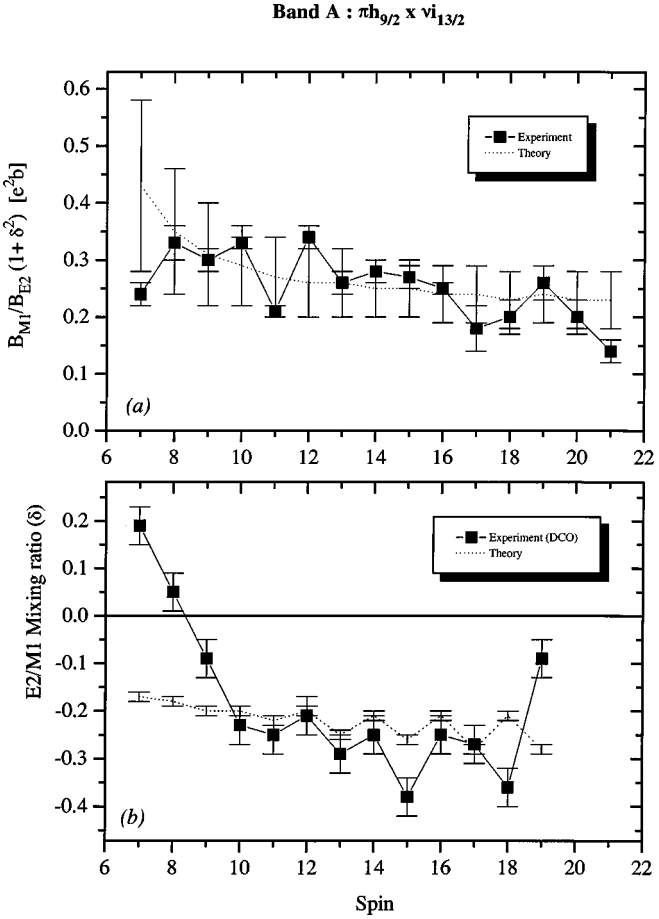

FIG. 5. (a) Theoretical two-quasiparticles-plus-rotor calculation of experimental branching ratios assuming that band A is based on the $\tilde{\pi}h_{9/2}\otimes\tilde{\nu}i_{13/2}$ coupling. (b) Same theoretical approach to experimental mixing ratios (see text).

$$E_{\mathrm{th}_{\mathrm{odd}}}(I,\vec{a})=\frac{1}{2\mathfrak{I}}\left[I(I+1)-\Omega^2+\langle j^{\perp 2}\rangle+\delta_{\Omega,\frac{1}{2}}a(-1)^{I+1/2}\times\left(I+\frac{1}{2}\right)\right]+\frac{1}{4\mathfrak{I}_1}(\mathfrak{I}-\mathfrak{I}_0)^2, \tag{9}$$

where Ω and $\sqrt{\langle j^{\perp 2}\rangle}$ are the absolute values of the projections of the angular momentum on the symmetry axis and on a plane orthogonal to it, respectively, of the odd particle and a is the decoupling parameter that multiplies the diagonal Coriolis term [13].

For a doubly odd nucleus the problem may be separated in five cases [2,3]: Normal; $K=\Omega_p-\Omega_n=0,\Omega_{p,n}\neq\frac{1}{2}$ (antiparallel coupling); compressed; semidecoupled (SDB), ($\Omega_{p(n)}>\frac{1}{2},\Omega_{n(p)}=\frac{1}{2}$); and doubly decoupled (DDB), ($\Omega_p=\Omega_n=\frac{1}{2}$) bands. The first two cases can be considered together by the expression

$$E_{o\text{-}o_{\mathrm{normal}}}=\frac{1}{2\mathfrak{I}}[I(I+1)-K^2+\langle j_p^{\perp 2}\rangle+\langle j_n^{\perp 2}\rangle]+\delta_{K,0}V_N(-1)^{I+1}+\frac{1}{4\mathfrak{I}_1}(\mathfrak{I}-\mathfrak{I}_0)^2, \tag{10}$$

TABLE V. Backbending (g to S) crossing frequencies estimated as the value of ω at which a change of slope of the experimental Routhians occurs. ND stands for the cases in which data were not available or insufficient.

Band	$\hbar\omega_c$ (MeV)		Band	$\hbar\omega_c$ (MeV)	
g.s.	^{168}Yb	0.28			
	^{169}Lu	^{171}Lu		^{169}Yb	^{171}Hf
$h_{9/2}$ (f)	0.30	0.27	$i_{13/2}$ (f)	0.34	0.36
$\frac{7}{2}^+[404]$ (f)	0.24	$\geqslant 0.24$, $\leqslant 0.28$	$i_{13/2}$ (uf)	0.32	0.34
$\frac{7}{2}^+[404]$ (uf)	0.23	$\geqslant 0.22$, $\leqslant 0.27$	$\frac{1}{2}^-[521]$ (f)	0.23	0.22
$\frac{1}{2}^+[411]$ (f)	0.23	0.20	$\frac{1}{2}^-[521]$ (uf)	>0.22	$\simeq 0.27$
$\frac{5}{2}^+[402]$	$\geqslant 0.21$	>0.20	$\frac{5}{2}^-[512]$	$\geqslant 0.19$, $\leqslant 0.23$	ND
$\frac{9}{2}^+[514]$ $(f+uf)$	>0.22, <0.25	>0.19, <0.23			

	^{170}Lu	Candidate	Additivity
Band A (f)	0.39	$\tilde{\pi}h_{9/2}\otimes\tilde{\nu}i_{13/2}$	0.36
Band A (uf)	0.34		0.34
Band B (f)	0.30	$\tilde{\pi}\frac{9}{2}^-[514]\otimes\tilde{\nu}i_{13/2}$	0.28
Band B (uf)	0.28		0.29
Band C (f)	0.34	$\tilde{\pi}\frac{7}{2}^+[404]\otimes\tilde{\nu}i_{13/2}$	0.30
Band C (f)	0.35		0.29
Band $C2$ (f)	>0.20	$\tilde{\pi}\frac{5}{2}^+[402]\otimes\tilde{\nu}i_{13/2}$	0.26
Band $C2$ (uf)	$\simeq 0.29$		0.26
Band D (f)	0.24	$\tilde{\pi}h_{9/2}\otimes\tilde{\nu}\frac{1}{2}^-[521]$	0.25
Band D (uf)	0.29		0.29
Band E (f)	0.28	$\tilde{\pi}\frac{1}{2}^+[411]\otimes\tilde{\nu}i_{13/2}$	0.29
Band E (uf)	0.28		0.28
Band F (f)	0.25	$\tilde{\pi}\frac{7}{2}^+[404]\otimes\tilde{\nu}i_{13/2}$ (K=0)	0.30
Band F (uf)	>0.24, <0.32		0.29
Band G	>0.19	$\tilde{\pi}\frac{7}{2}^+[404]\otimes\tilde{\nu}\frac{1}{2}^-[521]$	$\geqslant 0.19$
Band H	>0.18	$\tilde{\pi}\frac{1}{2}^+[411]\otimes\tilde{\nu}i_{13/2}$	0.28
Band I	>0.19	$\tilde{\pi}\frac{9}{2}^-[514]\otimes\tilde{\nu}\frac{1}{2}^-[521]$	>0.18
Band J	>0.19	$\tilde{\pi}\frac{5}{2}^+[402]\otimes\tilde{\nu}\frac{5}{2}^-[512]$	>0.16

where $K_{<}^{>}=|\Omega_p\pm\Omega_n|$ depending whether parallel or antiparallel coupling is going to be analyzed and V_N is the Newby-shift matrix element [15]. For SDB an explicit expression for the energy levels can be extracted by the diagonalization of a 2×2 Hamiltonian matrix that mixes two bands, one with $K_>=\Omega_{p(n)}+\frac{1}{2}$ and the other with $K_<=\Omega_{p(n)}-\frac{1}{2}$, by means of a nondiagonal Coriolis term of the form [8]

$$E_{\mathrm{Cor}}(I,\vec{a})=\langle K_>|\hat{H}_{\mathrm{cor}}|K_<\rangle=-\frac{1}{2}\left(\frac{1}{2\Im_>}+\frac{1}{2\Im_<}\right)\times a[(I-K_<)(I+K_<+1)]^{1/2}, \quad (11)$$

where a is the decoupling parameter associated to the $\Omega_{n(p)}=\frac{1}{2}$ state and $\Im_{<}^{>}$ are extracted using Eq. (7) and the value of $\langle\hat{R}^2\rangle$ calculated by

$$\langle\hat{R}^2\rangle_{<}^{>}=\sqrt{I(I+1)-K_{<}^{2}+\langle j_p^{\perp^2}\rangle+\langle j_n^{\perp^2}\rangle}. \quad (12)$$

The lowest eigenvalue leads to the final expression for the yrast energy levels:

$$E_{\mathrm{th_{sdb}}}(I,\vec{a})=\frac{E_>+E_<+\Delta V_{\mathrm{pn}}}{2}-\sqrt{\left(\frac{E_>-E_<+\Delta V_{\mathrm{pn}}}{2}\right)^2-E_{\mathrm{Cor}}^2}, \quad (13)$$

where ΔV_{pn} is the difference in the proton-neutron residual interaction strength between the $K_<$ and the $K_>$ bands and

$$E_{<}^{>}(I,\vec{a})=\frac{1}{2\Im_{<}^{>}}[I(I+1)-K_{<}^{2}+\langle j_p^{\perp^2}\rangle+\langle j_n^{\perp^2}\rangle]+\frac{1}{4\Im_1}(\Im_{<}^{>}-\Im_0)^2. \quad (14)$$

For a DDB an analog 2×2 Hamiltonian matrix can be constructed considering the $K_>=1$ and $K_<=0$ bands formed by

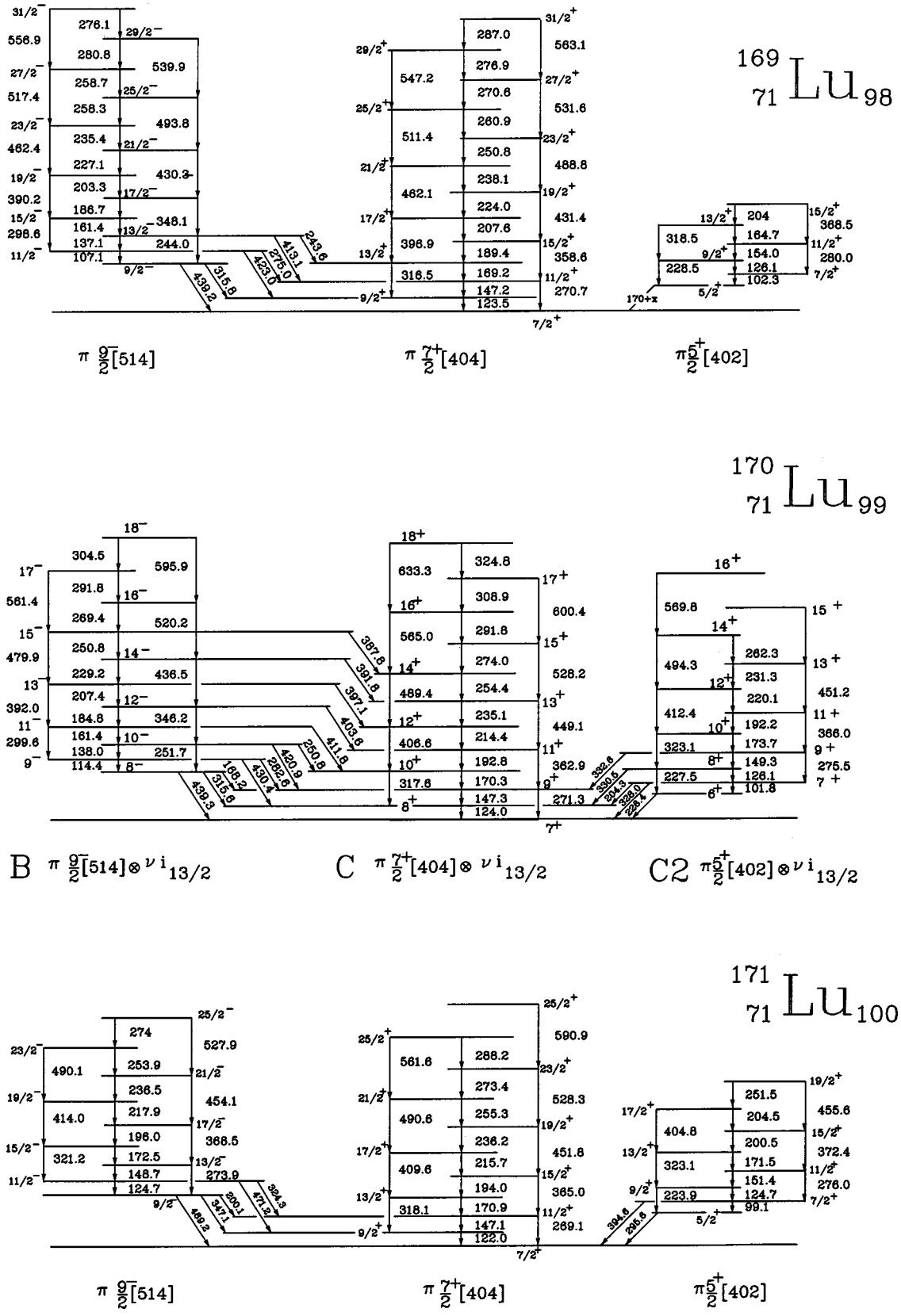

FIG. 6. Comparison of the $\tilde{\pi}\frac{9}{2}^{-}[514]$, $\tilde{\pi}\frac{7}{2}^{+}[404]$, and $\tilde{\pi}\frac{5}{2}^{+}[402]$ bands in ^{169,171}Lu with bands *B*, *C*, and *C*2 in ^{170}Lu. In spite of the fact that data for odd nuclei are available in the literature [20,21] the energy values obtained in the present work have been adopted for consistency.

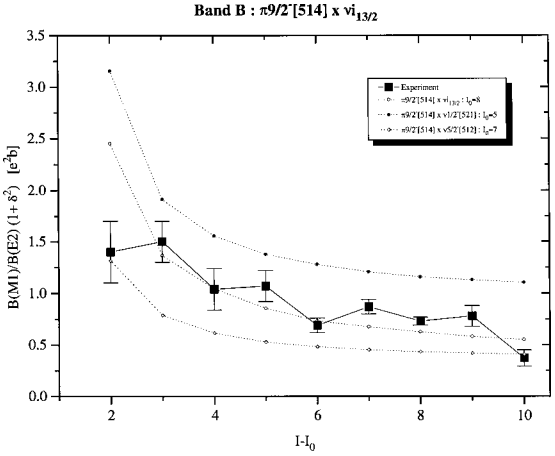

FIG. 7. Comparison of theoretical and experimental branching ratios for band B for three possible configurations. The best fit is obtained for $\pi\frac{9}{2}^-[514]\otimes\nu i_{13/2}$.

the coupling of two $\Omega=\frac{1}{2}$ orbits that will be mixed by a nondiagonal Coriolis term of the form [4]

$$E_{\mathrm{cor}}(I,\vec{a})=\langle K=1|\hat{H}_{\mathrm{cor}}|K=0\rangle=-\frac{1}{2}\left(\frac{1}{2\Im_{K=1}}+\frac{1}{2\Im_{K=0}}\right)\times[a_p+(-1)^{I+1}a_n]\sqrt{I(I+1)}, \quad (15)$$

where a_p and a_n are, respectively, the proton and neutron decoupling parameters and the moments of inertia $\Im_{K=1,0}$ are extracted by the procedure described above. The expression of the level energies has the same form of Eq. (13), where the diagonal matrix elements are calculated in analogy to the SDB case [Eq. (14)] with the addition of a Newby shift to the component $E_<=E_{K=0}$. The described model has, in spite of its simplicity, already several parameters, and some of them have to be held constant in the fits in order to achieve convergence. The values for $\langle j_{p,n}^{\perp\,2}\rangle$ were extracted from a Nilsson model calculation using the deformation parameter of the even-even ^{168}Yb core and the Nilsson parameters of Ref. [29] (see Table IV). The main advantage of this model is that it explicitly includes quantum effects, which modify the behavior of the rotational structure at low spins.

B. Band *A*

This is a very well-known structure [24,30] characterized as a semidecoupled band. The early onset of the characteristic dipolar staggering, the series of very low-energy transitions, and the very low $K_1=1.1$ [3,4] lead us to assign this band to the $\tilde{\pi}h_{9/2}\otimes\tilde{\nu}i_{13/2}$ configuration. A very good agreement is achieved between experimental data and theoretical predictions of the VMI-2QPR model both for branching ratios and δ mixing coefficients calculated with a diagonalization in the $\tilde{\pi}h_{9/2}\otimes\tilde{\nu}i_{13/2}$ configuration space. These results are summarized in Figs. 5(a) and 5(b). Furthermore, a striking additivity is observed in the inertia parameters, as seen in Table VI. Favored states have even spins ($\alpha=0$, α is the signature) up to high-spin values where a change of phase is produced. This is contrary to the expected [1–4] favored signature in the odd-odd nucleus (α_{p-n}^f) corresponding to the coupling between the favored signature of both proton (α_p^f) and neutron (α_n^f) orbitals, that for the $\tilde{\pi}h_{9/2}\otimes\tilde{\nu}i_{13/2}$ band would correspond to $\alpha_{p-n}^f=\alpha_p^f+\alpha_n^f=\frac{1}{2}+\frac{1}{2}=1$ (odd spin values). This situation has been recently described [31,32,24] and was explained in terms of a residual proton-neutron interaction. As occurs systematically [30] with this configuration a notorious delay of the back-bending crossing frequency (ω_c) is observed and is reproduced using the additivity rules (see Table V).

C. Band *B*

This band together with bands C, $C2$, and their linking transitions closely resemble the odd-proton $\tilde{\pi}\frac{9}{2}^-[514], \tilde{\pi}\frac{7}{2}^+[404], \tilde{\pi}\frac{5}{2}^+[402]$ structures in the neighboring odd-proton nuclei (see Fig. 6). This striking similarity does not only concern in-band transitions but also relative band-head excitation energies. The participation of $\tilde{\pi}\frac{9}{2}^-[514]$ in band B is strongly suggested by this analogy leaving three possible couplings for this band as discussed below (the coupling to the three lowest neutron excitations, namely $\tilde{\pi}\frac{9}{2}^-[514]\otimes\tilde{\nu}i_{13/2}$, $\tilde{\pi}\frac{9}{2}^-[514]\otimes\tilde{\nu}\frac{1}{2}^-[521]$ and $\tilde{\pi}\frac{9}{2}^-[514]\otimes\tilde{\nu}\frac{5}{2}^-[512]$, see Table III). The calculated branching ratios (using $N=5$ and $N=6$ shells for protons and neutrons, respectively) when compared with the experimental ones favor the $\tilde{\pi}\frac{9}{2}^-[514]\otimes\tilde{\nu}i_{13/2}$ configuration (see Fig. 7). A small delay of ω_c is expected by additivity and is in fact observed (see Table V), so the participation of the $i_{13/2}$ orbital is also preferred from this point of view. Furthermore, a systematic study of $E_{\gamma_{I+1\to I}}-E_{\gamma_{I\to I-1}}$ vs. I for the $\tilde{\pi}h_{11/2}\otimes\tilde{\nu}i_{13/2}$ configurations (the $\frac{9}{2}^-[514]$ orbital has $h_{11/2}$ parentage) shows a characteristic signature inversion at $I=12$ (see Fig. 8). Hence, the best candidate for band B is $\tilde{\pi}\frac{9}{2}^-[514]\otimes\tilde{\nu}i_{13/2}$. As a last additional argument Table VI shows that this configuration has the best additivity in the cranking parameters.

D. Band *C*

Once the configuration of band B has been established, the discussion of the previous section leads to $\tilde{\pi}\frac{7}{2}^+[404]\otimes\tilde{\nu}i_{13/2}$ for the intrinsic structure of band C. The predicted branching ratios fit well the experimental data. In this case $N=4$ was used for the proton orbital. Consistently, a notorious delay in ω_c (slightly greater that the one expected from additivity) is observed in Table V. Again good additivity of the inertia parameters is observed (see Table VI).

As already pointed out in the previous section this band and the one based on $\tilde{\pi}\frac{7}{2}^+[404]$ in the odd-proton neighboring isotopes have almost the same transition energies along a wide range of ω. This fact can be clearly seen in Fig. 9. Although the concept of twin bands is usually associated with identical bands, the extracted inertia parameters listed in Table VI show large differences with those extracted for the

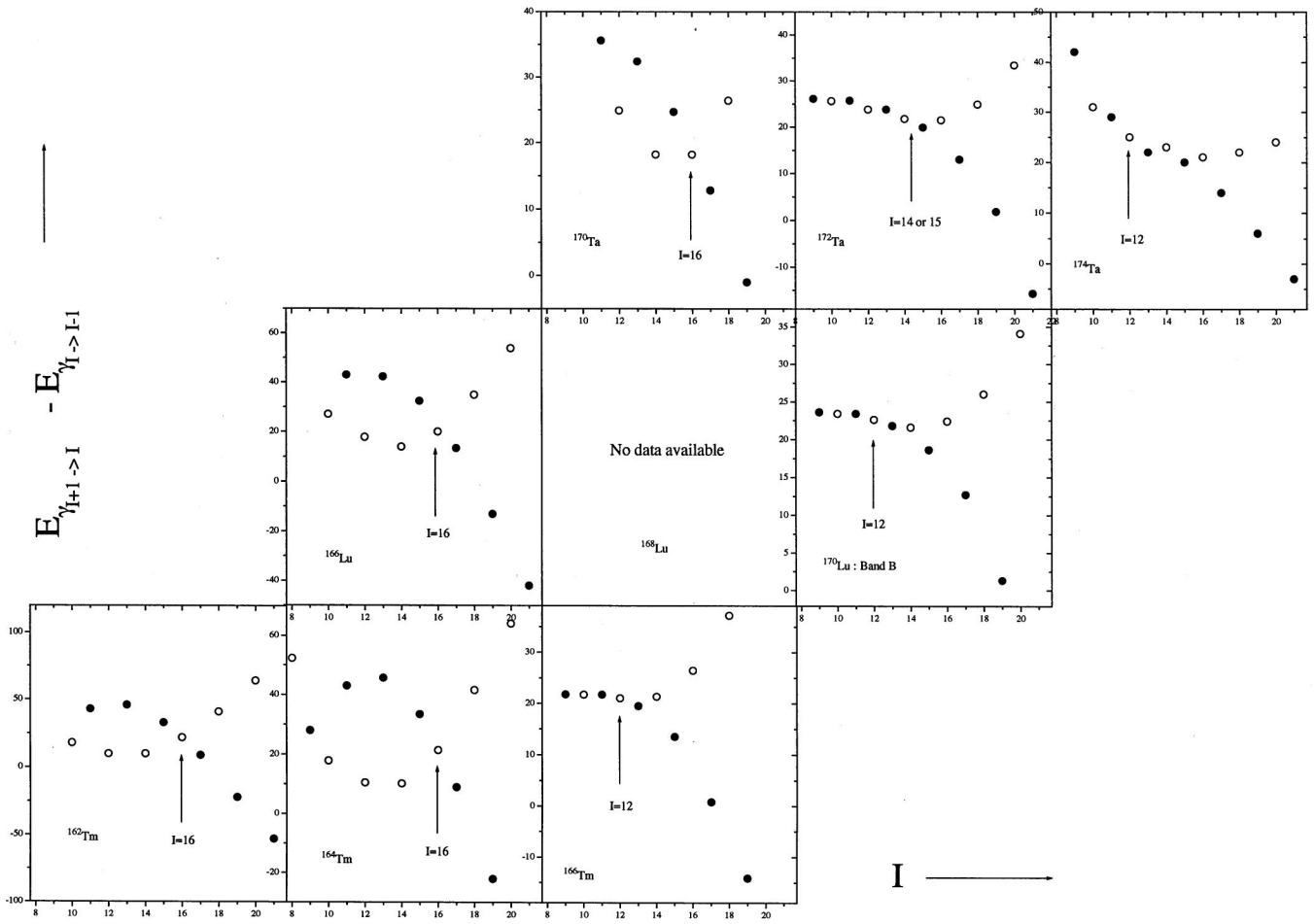

FIG. 8. Systematics of the difference in the energy of successive dipolar transitions against spin for the $\tilde{\pi}h_{11/2}\otimes\tilde{\nu}i_{13/2}$ band in the rare-earth region. The approximate spin at which a phase inversion occurs is indicated. Data were extracted from [23,39–42,33]. No data were available for ^{168}Lu.

$\tilde{\pi}\frac{7}{2}^{+}[404]$ band in ^{169}Lu and ^{171}Lu (see Table VII). An explanation of this phenomenon in terms of an accidental cancellation was suggested in Ref. [33].

E. Band *C*2

The configuration of this band follows immediately from the observation of Fig. 6 leading to the $\tilde{\pi}\frac{5}{2}^{+}[402]\otimes\tilde{\nu}i_{13/2}$ structure. The assignment is confirmed by the comparison of theoretical (using the same shells as with band *C*) and experimental branching ratios and the additivity of the inertia parameters (see Table VI). The backbending is slightly anticipated with respect to the core. This fact can be explained in terms of the additivity rule for ω_c because the $\tilde{\pi}\frac{5}{2}^{+}[402]$ orbits have a much earlier backbending that is partly compensated by the delay associated to the $\tilde{\nu}i_{13/2}$ orbital (see Table V).

F. Band *D*

The structure of this band corresponds unambiguously to the one characterized as doubly decoupled, which has been extensively discussed [4,5,27,34]. A fit to a VMI-2QPR model yields the decoupling parameters for the proton and neutron and a fairly good agreement is obtained with the ones extracted for the $\tilde{\pi}h_{9/2}$ proton excitation in the odd-*Z* neighboring isotopes ^{169,171}Lu and in ^{169}Yb and ^{171}Hf for the $\tilde{\nu}\frac{1}{2}^{-}[521]$ neutron excitation in the odd-*N* neighboring isotones (see Table VIII). Besides, a Newby shift was extracted yielding 36.8(8) keV which is very close to the theoretical value of 34 keV (calculated for the same configuration in ^{172}Lu in Ref. [35]). Moreover, a cranking fit of both signatures yields a difference of one unit in alignment as noted in Table VI and good additivity of the inertia parameters is observed. This band is then identified as $\tilde{\pi}h_{9/2}\otimes\tilde{\nu}\frac{1}{2}^{-}[521]$ (equivalently we can write $\tilde{\pi}h_{9/2}\otimes\tilde{\nu}\frac{1}{2}^{-}[\widetilde{420}]$ to recall explicitly the pseudospin nature of the neutron excitation [27]). In fact, this is the first case in which the lowest lying level of the doubly decoupled band is a 1^{+} (of rather pure $\tilde{\pi}\frac{1}{2}^{-}[541]\otimes\tilde{\nu}\frac{1}{2}^{-}[521]$, $K=0,1$ nature). This is related to the fact that the $\tilde{\pi}h_{9/2}$ structure evolves from the Ir isotopes where the lowest state is a $\frac{9}{2}^{-}$, through the Re isotopes where it is a $\frac{5}{2}^{-}$ to the odd Lu isotopes where the band-head corresponds to $\frac{1}{2}^{-}$ [34]. Based on our work and previous

TABLE VI. Inertia parameters $\Im_0$, $\Im_1$ and alignments i_0 calculated within the cranking model framework for each band using the first four quadrupole transitions above the level with spin $I=I_1$ and values resulting from additivity rules ($\Im_{o-o}=\Im_{\mathrm{odd}-Z}+\Im_{\mathrm{odd}-N}-\Im_{e-e}$, $i_{o-o}=i_{\mathrm{odd}-Z}+i_{\mathrm{odd}-N}-i_{e-e}$). The corresponding core and odd particle parameters are given in Table VII. On account of signature splitting effects only quadrupole sequences were considered and hence a separation into favored (f) and unfavored (uf) components was made.

Band	$^{(1)}\Im_0$	$^{(2)}\Im_1$	$i_0(\hbar)$	$\langle K^2\rangle$	I_1	Candidate	$\Im_0$ [a]	$\Im_1$ [b]	$i_0(\hbar)$
A (f)	59(1)	-90(20)	2.1(1)	12.5	6	$\tilde{\pi}h_{9/2}\otimes\tilde{\nu}i_{13/2}$	61(1)	-190(30)	2.8(1)
A (uf)	59(1)	-120(20)	2.0(1)	12.5	5	$\tilde{\pi}h_{9/2}\otimes\tilde{\nu}i_{13/2}$	61(2)	-200(40)	2.7(1)
B	61.7(9)	-180(60)	0.9(2)	64	8	$\tilde{\pi}\frac{9}{2}^-[514]\otimes\tilde{\nu}i_{13/2}$	61(1)	-180(20)	0.77(6)
	45.7(2)	-107(3)	0.53(2)	20.5	5	$\tilde{\pi}\frac{9}{2}^-[514]\otimes\tilde{\nu}\frac{1}{2}^-[521]$	51.7(5)	70(15)	0.48(3)
	56.8(7)	-125(15)	0.77(5)	49	7	$\tilde{\pi}\frac{9}{2}^-[514]\otimes\tilde{\nu}\frac{5}{2}^-[512]$	46.5(6)	-115(10)	0.21(2)
C	54.4(8)	-77(20)	0.7(1)	49	7	$\tilde{\pi}\frac{7}{2}^+[404]\otimes\tilde{\nu}i_{13/2}$	55(1)	-100(20)	0.66(6)
	39.7(4)	56(6)	0.03(4)	12.5	4	$\tilde{\pi}\frac{7}{2}^+[404]\otimes\tilde{\nu}\frac{1}{2}^-[521]$	45.2(4)	150(20)	0.37(2)
$C2$	55(2)	-110(40)	0.75(9)	36	6	$\tilde{\pi}\frac{5}{2}^+[402]\otimes\tilde{\nu}i_{13/2}$	55(3)	-150(60)	0.6(2)
D (f)	49.1(7)	95(10)	2.28(6)	0.5	5	$\tilde{\pi}h_{9/2}\otimes\tilde{\nu}\frac{1}{2}^-[521]$	51.3(7)	60(15)	2.5(1)
D (uf)	51.7(1)	8(2)	1.21(1)	0.5	4	$\tilde{\pi}h_{9/2}\otimes\tilde{\nu}\frac{1}{2}^-[521]$	48.7(7)	85(20)	1.9(1)
E (f)	54(2)	-26(24)	0.9(2)	12.5	5	$\tilde{\pi}\frac{1}{2}^+[411]\otimes\tilde{\nu}i_{13/2}$	54(2)	-60(50)	1.0(1)
E (uf)	56(2)	15(24)	0.5(1)	12.5	4	$\tilde{\pi}\frac{1}{2}^+[411]\otimes\tilde{\nu}i_{13/2}$	53(2)	-50(30)	1.1(1)
E (f)	53(2)	-16(21)	0.9(2)	6.5	5	$\tilde{\pi}h_{9/2}\otimes\tilde{\nu}\frac{5}{2}^-[512]$	46.1(7)	-80(10)	2.26(3)
E (uf)	54(1)	36(18)	0.7(1)	6.5	4	$\tilde{\pi}h_{9/2}\otimes\tilde{\nu}\frac{5}{2}^-[512]$	46.1(7)	-80(10)	2.26(3)
F (f)	59(2)	-120(40)	0.34(9)	0	2	$\tilde{\pi}\frac{7}{2}^+[404]\otimes\tilde{\nu}i_{13/2}$	55(1)	-100(20)	0.7(1)
F (uf)	52(2)	-6(20)	1.3(2)	0	5	$\tilde{\pi}\frac{7}{2}^+[404]\otimes\tilde{\nu}i_{13/2}$	55(2)	-100(30)	0.7(1)
G	46(1)	30(20)	0.2(1)	12.5	4	$\tilde{\pi}\frac{7}{2}^+[404]\otimes\tilde{\nu}\frac{1}{2}^-[521]$	45.2(4)	150(20)	0.37(2)
H	53(2)	100(60)	0.7(4)	12.5	4	$\tilde{\pi}\frac{1}{2}^+[411]\otimes\tilde{\nu}i_{13/2}$	53(2)	-60(50)	1.1(1)
H	49(3)	170(80)	0.3(1)	6.5	3	$\tilde{\pi}h_{9/2}\otimes\tilde{\nu}\frac{5}{2}^-[512]$	46.1(7)	-80(10)	2.26(3)
I	54.9(5)	-33(20)	0.53(3)	20.5	5	$\tilde{\pi}\frac{9}{2}^-[514]\otimes\tilde{\nu}\frac{1}{2}^-[521]$	52(1)	70(15)	0.48(3)
J	53.7(5)	34(22)	0.12(2)	25	5	$\tilde{\pi}\frac{5}{2}^+[402]\otimes\tilde{\nu}\frac{5}{2}^-[512]$	40(3)	-40(50)	0.0(2)

[a] In units of $\hbar^2\mathrm{MeV}^{-1}$.
[b] In units of $\hbar^2\mathrm{MeV}^{-3}$.

data the absolute band head energy of $\tilde{\pi}h_{9/2}\otimes\tilde{\nu}\frac{1}{2}^-[521]$ structure is likely to be 98.5 keV (against 73 keV predicted by the zero-order approximation, Table III). The here unobserved 16.3 keV , $3^+\rightarrow 1^+$, transition is accurately reproduced extrapolating the VMI-2QPR calculation with the parameters extracted by the fit (prediction is 14.5 keV) and had been in fact observed in Ref. [17].

G. Bands E and H

The accidental degeneracy at $I^\pi=8^+$ between bands D and E fixes the parity as positive and I_0 to 3 or 4. These bands are similar to the one based on the $\tilde{\nu}i_{13/2}$ odd neutron excitation in the neighboring odd-A, odd-N nuclei. The candidates for band E and H are then $[\tilde{\pi}\frac{1}{2}^+[411]\otimes\tilde{\nu}i_{13/2}]_{4^+,3^+}$ with aligned and antialigned pseudospin [27] coupling, respectively, which is a new case of a semidecoupled band [8] with a proton decoupling parameter that satisfies $|a_p|\sim 1$. As can be seen in Table VII the $\tilde{\pi}\frac{1}{2}^+[411]$ quasiparticle does not modify the moment of inertia of the even-even core. Under these conditions (if the difference in the value of the residual interaction for the $K_>$ and the $K_<$ components can be neglected) twin bands are predicted [8]. In fact, the transition energies of bands H and E are very similar among themselves and to the $\tilde{\nu}i_{13/2}$ band in ^{169}Yb. Agreement between experimental and semiclassically calculated branching ratios for band E is achieved for $I\simeq 8$, that is, when the effect

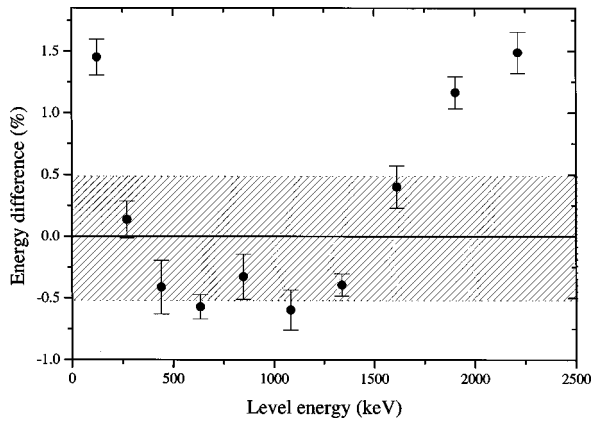

FIG. 9. Plot of the relative energy difference (in percentage) for corresponding γ rays in ^{170}Lu and ^{171}Lu as a function of the excitation energy of the emitting state in the odd-odd nucleus.

of the admixture with band *F* has been attenuated. The absence of a delay in ω_c can be attributed to a compensation of the delay produced by the $i_{13/2}$ orbital and the anticipation of the $\frac{1}{2}^+[411]$. Additivity of inertia parameters is observed for the $\frac{1}{2}^+[411]\otimes\tilde{\nu}i_{13/2}$ assignment and a VMI-2QPR fit yields a value for the proton decoupling parameter very near to the ones extracted from the odd neighbors (see Table VIII).

H. Band *F*

This structure has a remarkable dipolar staggering. Its appearance can only be attributed to the coupling of two $\Omega=\frac{1}{2}$ states (a DDB) or to the coupling to $K=0$ of two states with the same value of Ω, considering the inclusion of a splitting term in the Hamiltonian, namely the Newby shift. The degeneracy at $I=5$ (with band *E*) and the $M1/E2$ character of the linking transitions leave as the only possibility the $\tilde{\pi}\frac{7}{2}^+[404]\otimes\tilde{\nu}i_{13/2}(\frac{7}{2}^+[633])$ ($K=0$ band with positive parity). An expected delay of ω_c, due to the participation of the $i_{13/2}$ neutron orbital was observed only for the unfavored signature. The experimental branching ratios are in good agreement with the semiclassical approximation. Deviations are most likely due to admixture with band *E*. Good additivity of inertia parameters was found, as can be seen in Table VI. A Newby-shift corrected VMI-2QPR fit was done and the results are summarized in Table VIII and, as can be seen, the agreement with the theoretically predicted [35] $V_N=36$ keV value is striking. Finally, the band is completed when the 44.5 keV, $2^+\rightarrow 0^+$ transition, observed in [17], is added to the bottom of the scheme and the whole structure comprising bands *D*, *H*, *E*, and *F* is closed in itself.

I. Bands *G*, *I*, and *J*

The lack of linking transitions from or to these bands makes the determination of the structures ambiguous. The spins of the band heads are unknown and the presence of low-energy transitions below the observed ones cannot be ruled out. In addition, the lack of information of the high-spin portion of these bands only allowed a lower limit for the crossing frequencies. Band *J* shows dipolar staggering near the 173.0 keV transition. This phenomenon is observed for the $\tilde{\pi}\frac{5}{2}^+[402]$ band in the odd proton neighbors ^{169,171}Lu, which would suggest that this orbital is present in band *J*. There are two possible couplings left for $\tilde{\pi}\frac{5}{2}^+[402]$: One to $\tilde{\nu}\frac{1}{2}^-[521]$ and the other to $\tilde{\nu}\frac{5}{2}^-[512]$. The first one lies lower in energy according to the zero-order scheme while the

TABLE VII. Inertia parameters $\mathfrak{I}_0$, $\mathfrak{I}_1$ and alignments i_0 calculated within the cranking model framework for the ground state band in the even-even core and the single-particle band in the neighboring odd-*A* nuclei using the first four quadrupole transitions. On account of signature splitting effects only quadrupole sequences were considered and hence a separation into favored (*f*) and unfavored (uf) components was done. I_1 is the spin of the lowest level of the sequence.

Band	$\langle K^2\rangle$	I_1	Nucleus	$\mathfrak{I}_0$ [a]	$\mathfrak{I}_1$ [b]	$i_0(\hbar)$	Nucleus	$^{(1)}\mathfrak{I}_0$	$^{(2)}\mathfrak{I}_1$	$i_0(\hbar)$
g.s.	0	0	^{168}Yb	33.7(1)	138(6)	0.005(5)				
$\frac{7}{2}^+[404]$	12.25	3.5	^{169}Lu	34.5(3)	168(5)	0.07(2)	^{171}Lu	36.2(2)	80(5)	0.02(2)
$\frac{9}{2}^-[514]$	20.25	4.5		39(2)	90(40)	0.7(1)		42.2(3)	15(5)	0.13(2)
$\frac{5}{2}^+[402]$	6.25	2.5		33(2)	160(60)	0.0(2)		36(2)	70(40)	-0.1(1)
$\frac{1}{2}^+[411]$	0.25	0.5		36(2)	170(40)	-0.3(2)		37.0(6)	110(10)	-0.33(4)
$\frac{1}{2}^+[411]$	0.25	1.5		33(1)	240(20)	0.49(8)		34.4(6)	150(10)	0.44(5)
$\frac{1}{2}^-[541]$	1.25	2.5		40.1(9)	90(10)	2.10(9)		42.0(4)	30(5)	2.21(3)
$\frac{1}{2}^-[541]$	1.25	1.5		47(2)	115(35)	-0.9(2)		56.1(4)	-30(7)	- 1.65(3)
$\frac{7}{2}^+[633]$	12.25	3.5	^{169}Yb	54(1)	-100(25)	0.44(6)	^{171}Hf	52(2)	-110(40)	0.9(1)
$\frac{7}{2}^+[633]$	12.25	4.5		53.0(6)	-110(10)	0.59(4)		52(1)	-50(20)	1.0(1)
$\frac{1}{2}^-[521]$	0.25	0.5		43.3(1)	160(10)	0.33(1)		39.3(4)	250(20)	0.35(2)
$\frac{1}{2}^-[521]$	0.25	1.5		41.0(1)	170(10)	-0.29(1)		37.8(3)	230(10)	-0.26(2)
$\frac{5}{2}^-[512]$	6.25	2.5		38.4(1)	16(1)	0.06(1)		35.6(3)	175(10)	0.10(2)

[a] In units of $\hbar^2\text{MeV}^{-1}$.
[b] In units of $\hbar^2\text{MeV}^{-3}$.

TABLE VIII. (a) Parameters calculated within the VMI-2QPR framework for doubly decoupled (DDB), semidecoupled (SDB), and Newby-shifted (NB) bands. In the cases the experimental error is not specified the parameter has been fixed for the fit. (b) Parameters calculated within the VMI-1QPR framework for $\Omega = 1/2$ bands in odd-A nuclei.

Band	Model	$\Im_0$ [a]	$\Im_1$ [b]	a_p	a_n	ΔV_{pn} [c]	V_N [c]
A $(\tilde{\pi}h_{9/2}\otimes\tilde{\nu}i_{13/2})$	SDB	59(5)	-30(100)	$\pm$4.0(5)		0	
D $(\tilde{\pi}h_{9/2}\otimes\tilde{\nu}\frac{1}{2}^-[521])$	DDB	52.1(5)	-1(14)	$\pm$3.30(4)	$\mp$0.892(6)		36.8(8)
$E+H$ $(\tilde{\pi}\frac{1}{2}^+[411]\otimes\tilde{\nu}i_{13/2}$ $(f+uf))$	SDB	61.0(8)	-178(33)	$\pm$1.25(3)		79(7)	
F $(\tilde{\pi}\frac{7}{2}^+[404]\otimes\tilde{\nu}i_{13/2})$	NB	64(4)	-80(50)				40(4)
G $(\tilde{\pi}\frac{7}{2}^+[404]\otimes\tilde{\nu}\frac{1}{2}^-[521])$	SDB	42(7)	70(150)		$\pm$1.6(7)	70	
I $(\tilde{\pi}\frac{9}{2}^-[514]\otimes\tilde{\nu}\frac{1}{2}^-[521])$	SDB	53(3)	-4(47)		$\pm$1.6(7)	-6(83)	
$\tilde{\pi}h_{9/2}$ (^{169}Lu) [20]		42.8(6)	32(18)	+3.80(6)			-
$\tilde{\pi}h_{9/2}$ (^{171}Lu) [21]		44.2(6)	-15(15)	+4.20(6)			
$\tilde{\pi}\frac{1}{2}^+[411]$ (^{169}Lu)		30(1)	260(30)	-1.0(1)			
$\tilde{\pi}\frac{1}{2}^+[411]$ (^{171}Lu)		32.7(7)	170(20)	-0.94(7)			
$\tilde{\nu}\frac{1}{2}^-[521]$ (^{169}Yb) [43]		40.9(1)	200(10)		+0.80(1)		
$\tilde{\nu}\frac{1}{2}^-[521]$ (^{171}Hf) [44]		36.1(4)	290(10)		+0.84(2)		

[a]In units of $\hbar^2$MeV^{-1}.
[b]In units of $\hbar^2$MeV^{-3}.
[c]In units of keV.

second has greater spins. The $K_1=4.49$ of band J favors the second assignment and so it does the comparison of experimental and calculated branching ratios (see Fig. 10).

The strong dipolar cascade of band I can be associated with the presence of the $\frac{9}{2}^-[514]$ orbital. This is consistent with the $B(M1)/B(E2)$ calculation and observed in the odd proton neighbors. If the 94.6 keV transition is taken as in-band one obtains $K_1=3.63$, which would imply a certain degree of compression. On the other hand, the mentioned transition might be considered as out of band, leading to $K_1=4.68$ which can be interpreted as the mixing of two states with $K_{>(<)}=5(4)$. The candidate for this band is $\tilde{\pi}\frac{9}{2}^-[514]\otimes\tilde{\nu}\frac{1}{2}^-[521]$. The possible assignments for band G are $\tilde{\pi}\frac{7}{2}^+[404]\otimes\tilde{\nu}\frac{1}{2}^-[521]$, $\tilde{\pi}h_{9/2}\otimes\tilde{\nu}\frac{5}{2}^-[512]$, and $\tilde{\pi}\frac{1}{2}^+[411]\otimes\tilde{\nu}\frac{5}{2}^-[512]$, which are cases of semidecoupled bands. The $K_1=3.78$ favors the first assignment since the band head has to be considered as the admixture of two states with $K_{>(<)}=4(3)$. An interesting point is that this band is not twinned to the neighboring $\tilde{\pi}\frac{7}{2}^+[404]$ excitations. This fact can be explained by the change in moment of inertia due to the participation of the neutron. In this region it can be seen that the ''twin-band'' condition is gradually lost starting from the striking twin pair ^{174}Lu-^{175}Lu when moving to lower mass numbers [20,21,36–38]. The case of band G in

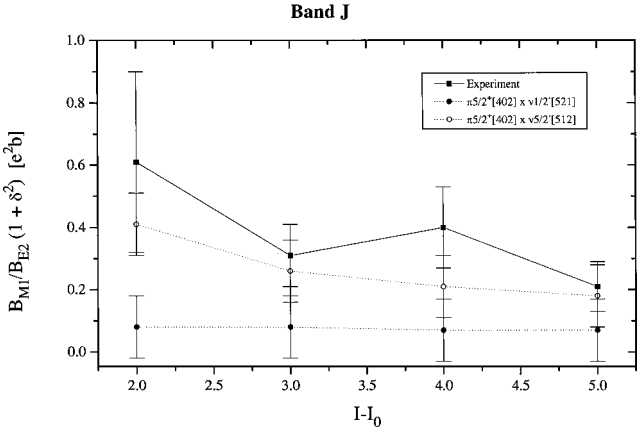

FIG. 10. Comparison of theoretical and experimental branching ratios for band J for two possible configurations. The best fit is obtained assigning the $\pi\frac{5}{2}^+[402]\otimes\nu\frac{5}{2}^-[512]$.

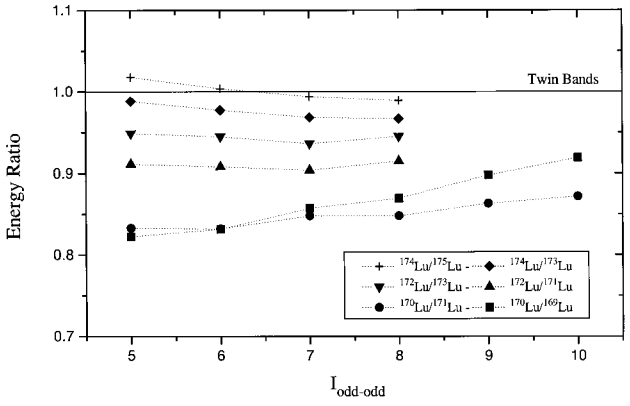

FIG. 11. Systematics of the successive corresponding transition energy ratios $S(I_{o-o})=(E^{o-o}_{I_{o-o}}-E^{o-o}_{I_{o-o}-1})/(E^{o}_{I_{o-o}-\frac{1}{2}}-E^{o}_{I_{o-o}-\frac{3}{2}})$ for odd (o) and doubly odd ($o-o$) Lu isotopes. Data were taken from Refs. [20,21,36–38]. The energy ratio 1.0 corresponds to twin bands.

^{170}Lu follows the systematics and the large differences in corresponding transition energies should not be surprising. This analysis is clearly reflected in Fig. 11.

IV. SUMMARY AND CONCLUSIONS

The doubly odd nucleus ^{170}Lu has been studied through state-of-the-art γ-ray spectroscopic techniques and the yrast band structure scheme has been determined comprising 11 rotational bands. Using the coupling schemes proposed in Ref. [3] for doubly-odd nuclei and all the systematics accumulated so far, eight bands were unambiguously assigned while the others have more tentative character. This systematic analysis seems to point to a case of twin bands in the normal deformation regime that happen to be nonidentical, that is, have very different inertia parameters. In fact, the difference of almost 40% in $\mathfrak{I}_0$ is strongly contrasting with the slight difference in the transition energies of about 0.5%, only found in superdeformed twin bands. This phenomenon cannot be explained just in terms of a pure rotor, nor resorting to the pseudospin symmetry. On the other hand, a cranking-model-based mechanism of accidental cancellation of the differences in spin and variable moments of inertia resulting in small differences in transition energies has been proposed [33], stating that

$$E_\gamma \simeq \frac{\Delta I_x R}{\mathfrak{I}^{(1)}}, \tag{16}$$

where ΔI_x is the difference in transverse angular momentum, $R = I_x - i_0$ is the collective angular momentum, and $\mathfrak{I}^{(1)}$ is the cinematic moment of inertia. The factor ΔI_x is larger in the doubly odd than in the odd nucleus, and since $\mathfrak{I}^{(1)}_{o\text{-}o} > \mathfrak{I}^{(1)}_{o}$, the three factors must balance each other to achieve identical transition energies E_γ. However, such small differences in transition energies along a relatively wide range of ω are difficult to understand in terms of a cancellation that is more likely to be localized in ω, taking into account its fortuitous character.

In addition, the set of favored and unfavored components of band $\tilde{\pi}\frac{1}{2}^+[411]\otimes\tilde{\nu}i_{13/2}$ agree with the prediction of [8]. In this case, however, the facts that $|a_p| \neq 1$, that the residual interaction cannot be neglected and that there is a distortion due to the admixture with other configurations imply that a too striking similarity should not be expected. On the other hand, the observed similarity in this case is consistent with the fact that the contribution of the decoupled particle to the moment of inertia is negligible (see parameters of $\frac{1}{2}^+[411]$ bands in Tables VII and VIII), hence leading to identical twin bands.

[1] A. J. Kreiner, M. Fenzl, S. Lunardi, and M. A. J. Mariscotti, Nucl. Phys. **A282**, 243 (1977).

[2] A. J. Kreiner, J. Davidson, M. Davidson, D. Abriola, C. Pomar, and P. Thieberger, Phys. Rev. C **36**, 2309 (1987); **37**, 1338 (1988).

[3] A. J. Kreiner, in *Proceedings of the International Conference on Contemporary Topics in Nuclear Structure Physics*, Cocoyoc, Mexico, 1988, edited by R. F. Casten, A. Frank, M. Moshinsky, and S. Pittel (World-Scientific, Singapore, 1988), p. 521, and references therein.

[4] A. J. Kreiner, D. Di Gregorio, A. J. Fendrik, J. Davidson, and M. Davidson, Phys. Rev. C **29**, R1752 (1984); Nucl. Phys. **A432**, 451 (1985).

[5] A. J. Kreiner, J. Davidson, M. Davidson, P. Thieberger, E. K. Warburton, S. André, and J. Genevey, Nucl. Phys. **A489**, 525 (1988).

[6] A. J. Kreiner and M. A. J. Mariscotti, Phys. Rev. Lett. **43**, 1150 (1979).

[7] A. J. Kreiner and M. A. J. Mariscotti, J. Phys. G **6**, 13 (1980).

[8] A. J. Kreiner, Phys. Rev. C **38**, R2486 (1988).

[9] T. Byrski, F. A. Beck, D. Curien, C. Schuck, P. Fallon, A. Alderson, I. Ali, M. A. Bentley, A. M. Bruce, P. D. Forsyth, D. Howe, J. W. Roberts, J. F. Sharpey-Schafer, G. Smith, and P. J. Twin, Phys. Rev. Lett. **64**, 1650 (1990).

[10] W. Nazarewicz, P. J. Twin, P. Fallon, and J. D. Garret, Phys. Rev. Lett. **64**, 1654 (1990).

[11] G. Levinton *et al.*, LNL-INFN (Rep) 105/96 p. 74 (1996).

[12] A. J. Kreiner and D. Hojman, Phys. Rev. C **36**, 2173 (1987).

[13] A. Bohr and B.R. Mottelson in *Nuclear Structure* (Benjamin, Reading, MA, 1975), Vol. 2.

[14] M. A. J. Mariscotti, G. Scharff-Goldhaber, and B. Buck, Phys. Rev. **178**, 1864 (1969).

[15] N. D. Newby, Phys. Rev. **125**, 2063 (1962).

[16] D. Bazzacco, in Proceedings of the International Conference on Nuclear Structure at High Angular Momentum, Ottawa 1992 [Report No. AECL 10613 (unpublished)]; Vol. 2, p. 376.

[17] J. Treherne, J. Vanhorenbeeck, and J. Valentin, Nucl. Phys. **A131**, 193 (1969).

[18] D. C. Camp and F. M. Bernthad, Phys. Rev. C **6**, 1040 (1972).

[19] V. S. Shirley, Nucl. Data Sheets **58**, 871 (1989).

[20] C. Foin, D. Barnéoud, S. A. Hjorth, and R. Berthoux, Nucl. Phys. **A199**, 129 (1973).

[21] P. Kemnitz, L. Funke, K. H. Kaun, H. Sodan, G. Winter, and M. I. Baznat, Nucl. Phys. **A209**, 271 (1973).

[22] Chr. Bargholtz and P. E. Tegnér, Nucl. Instrum. Methods Phys. Res. A **256**, 513 (1987).

[23] D. Hojman, A. J. Kreiner, M. Davidson, J. Davidson, M. E. Debray, E. W. Cybulska, P. Pascholatti, and W. A. Seale, Phys. Rev. C **45**, 90 (1992).

[24] M. A. Cardona, A. J. Kreiner, D. Hojman, G. Levinton, M. E. Debray, M. Davidson, J. Davidson, R. Pirchio, H. Somacal, D. R. Napoli, D. Bazzacco, N. Blasi, R. Burch, D. De Acuña, S. M. Lenzi, G. Lo Bianco, J. Rico, and C. Rossi Alvarez, Phys. Rev. C **59**, 1298 (1999).

[25] C. J. Gallagher, Jr. and S. A. Moszkowski, Phys. Rev. **111**, 1282 (1958).

[26] S. H. Harris, Phys. Rev. **138**, B509 (1965).

[27] A. J. Kreiner, M. A. Cardona, H. Somacal, M. E. Debray, D. Hojman, J. Davidson, M. Davidson, D. De Acuña, D. R.

Napoli, J. Rico, D. Bazzacco, R. Burch, S. M. Lenzi, C. Rossi Alvarez, N. Blasi, and G. Lo Bianco, Phys. Rev. C **50**, R530 (1994).
[28] S. G. Nilsson, K. Dan. Viden. Selsk. Mat. Fys. Medd. **29**, 16 (1955).
[29] J. P. Davidson in *Collective Models of the Nucleus* (Academic, New York, 1968).
[30] A. J. Kreiner, Nucl. Phys. **A520**, 225c (1990).
[31] R. A. Bark, J. M. Espino, W. Reviol, P. B. Semmes, H. Carlsson, I. G. Bearden, G. B. Hagemann, H. J. Jensen, I. Ragnarsson, L. L. Riedinger, H. Ryde, and P. O. Tjom, Phys. Lett. B **406**, 193 (1997).
[32] R. A. Bark, H. Carlsson, S. J. Freeman, G. B. Hagemann, F. Ingebretsen, H. J. Jensen, T. Lönnroth, M. J. Piiparinen, I. Ragnarsson, H. Ryde, H. Schnack-Petersen, P. B. Semmes, and P. O. Tjom, Nucl. Phys. **A630**, 603 (1998).
[33] D. Hojman, A. J. Kreiner, and M. Davidson, Phys. Rev. C **46**, 1203 (1992).
[34] J. Davidson, M. Davidson, M. E. Debray, G. Falcone, D. Hojman, A. J. Kreiner, I. Mayans, C. Pomar, and D. Santos, Z. Phys. A **324**, 363 (1986).
[35] H. Frisk, Z. Phys. **A330**, 241 (1988).
[36] B. Singh, Nucl. Data Sheets **75**, 199 (1995).
[37] A. Bruder, S. Drissi, V. A. Ionescu, J. Kern, and J. P. Vorlet, Nucl. Phys. **A474**, 518 (1987).
[38] P. Skensved, R. Chapman, R. L. Kozub, J. R. Leslie, W. McLatchie, D. Ward, H. R. Andrews, and O. Häusser, Nucl. Phys. **A366**, 125 (1981).
[39] S. Drissi, J. Cl. Dousse, V. Ionescu, J. Kern, J. A. Pinston, and D. Barnéoud, Nucl. Phys. **A466**, 385 (1987).
[40] S. J. Mannanal, B. Boschung, M. W. Carlen, J. Cl. Dousse, S. Drissi, P. E. Garrett, J. Kern, Ch. Rhême, J. P. Vorlet, C. Günthe, J. Manns, and U. Müller, Nucl. Phys. **A582**, 141 (1995).
[41] J. C. Bacelar, R. Chapman, J. R. Leslie, J. C. Lisle, J. N. Mo, E. Paul, A. Sincock, J. C. Willmott, J. D. Garrett, G. B. Hagemann, B. Herskind, A. Holm, and P. M. Walker, Nucl. Phys. **A442**, 547 (1985).
[42] D. Hojman *et al.* (unpublished).
[43] V. S. Shirley, Nucl. Data Sheets **64**, 505 (1991).
[44] G. D. Dracoulis and P. M. Walker, Nucl. Phys. **A330**, 186 (1979).